ABSTRACT

Non-Destructive Inspection Approach Using Ultrasound to Identify the Material State and Internal Temperature for Amorphous and Semi-Crystalline Materials

Elliott W. Jost

Director: David Jack, Ph.D.

Many invasive techniques exist to identify the temperature and phase of a semi-crystalline material. Most current methods require physical contact or implicit techniques utilizing light reflectance of the specimen. This work presents an ultrasonic nondestructive inspection approach that circumvents these disadvantages to identify phase change regions and infer a material's internal temperature. An experiment is constructed and performed to capture the ultrasonic characteristics of a wax as it undergoes melting and subsequent cooling. Results show a clear relationship between material speed of sound and temperature. This thesis demonstrates the range of temperature over which the semi-crystalline material melts is readily identified by the speed of sound represented as a function of material temperature. The investigated ultrasonic NDE method has direct applications in many industries, including oil and gas, food and beverage, and polymer matrix composites, Specifically, the method has many implications for expanding current capabilities of nondestructive inspection of multi-phase materials.

APPROVED BY DIRECTOR OF HONORS THESIS:

_____

Dr. David Jack, Department of Mechanical Engineering

APPROVED BY THE HONORS PROGRAM:

_____

Dr. Elizabeth Corey, Director

DATE: _____

NON-DESTRUCTIVE INSPECTION APPROACH USING ULTRASOUND TO IDENTIFY THE MATERIAL STATE AND INTERNAL TEMPERATURE FOR AMORPHOUS AND SEMI-CRYSTALLINE MATERIALS

A Thesis Submitted to the Faculty of

Baylor University

In Partial Fulfillment of the Requirements for the

Honors Program

By

Elliott Jost

Waco, Texas

May 2018

TABLE OF CONTENTS

LIST OF FIGURES

ACKNOWLEDGMENTS

Firstly, I would like to thank my advisor, Dr. David Jack, for your support and encouragement throughout the research process. You have been a source of wisdom and direction and I will be forever grateful for the passion for engineering and learning you have helped instill in me. The opportunities you have given me—from conference trips to having my own research project—have cemented my desire to pursue engineering research as a career.

To my parents, I would like to say thank you for the love and encouragement you have provided me. Both of you have always supported me and helped me in everything I have done, regardless of the outcome. Thank you for the continual love and guidance.

To my friends, thank you for sharing this journey with me. I will always be thankful for your friendship and the memories we have shared at Baylor. The thesis process would have been impossible without you.

Lastly, to the members of the Sic ‘Em research group, thank you for taking me in as one of your own. Each of you have helped make the past two years an absolute blast.

CHAPTER ONE:

INTRODUCTION

1.1 Research Motivation and Objective

At present, many methods of phase identification and temperature measurement are known. Many of these methods, however, require physical contact or visual line-of-sight to properly measure temperature. Examples of this are traditional thermocouples, which require physical contact, and infrared thermography, which requires a visual line-of-sight with the material. Infrared thermography in particular is limited to measuring only surface temperatures and is susceptible to inaccuracies due to calibration errors related to emissivity values. In the present study an automated ultrasound experiment was performed on a soy-based wax to develop techniques to non-invasively measure in real-time the internal temperature and detect phase changes. Multiple techniques were developed which identify the melt and solidification time and temperature of EcoSoya wax. By characterizing the speed of sound versus temperature relationship of EcoSoya wax, a two-dimensional imaging technique was developed for identifying phase regions in the wax in real time.

This research has applications in a variety of industries including oil and gas, food and beverage, and polymer composites for quality control, process monitoring, and system control. One such envisioned application of real-time, internal, non-invasive temperature monitoring in the oil and gas field is using ultrasonics to monitor the curing of cement in-situ as it solidifies. Oil tie-back wells, common in the oil and gas industry,

need to be poured and cured quickly. With the ability to use ultrasonic sensors to monitor temperature and other indicators of cure, the turn-around time between sections could be reduced in these wells, ultimately resulting in saved dollars for drillers.

Similarly, applications in the food and beverage processing industry relate to using ultrasound to measure the material phase state of candies and beverages during manufacturing. For example, chocolate is required to maintain a specified constituency during processing which is indicative of its taste characteristics. By monitoring the chocolate melt in a pipe in real-time, efficiency could be improved. Researchers have already been exploring the use of ultrasound for improved chocolate making [1–3]. Additionally, the proposed non-invasive technique provides for increased safety and sanitation standards to be met.

Many applications in the polymer composites industry could benefit significantly from the proposed monitoring system. Injection molding, a process which involves injecting a liquid thermoplastic into a shaped mold to cool into a final shape, could use ultrasonic temperature measurement for improving part quality and decreasing cycle time. Screw extruders, which melt polymers to be extruded into a designated shape, could also benefit from this type of process control. Through the installation of ultrasonic sensors in molds or extruders, temperature and phase of cooling parts could be monitored [4,5]. This would result in an intimate knowledge of the cooling process and allow for stronger parts to be made more efficiently. Additionally, improved thermoplastic cure monitoring could be realized, which has many applications in the automotive and aerospace industries. Because of the high use of injection molding, extrusion, and thermoplastic applications in the polymer composites industry, the proposed ultrasonic

monitoring technique could directly impact the automotive and aerospace industries by providing higher-quality parts at a lower cost.

1.2 Thesis Overview

This thesis will begin with a literature review of current work in ultrasonic temperature measurement in Chapter 2. Current applications for ultrasonic temperature measurement will be discussed, which will provide a context for understanding of the contribution of the current work. Then, in Chapter 3, an introduction to ultrasonic theory will be presented. Following this, results from the current work will be presented and discussed in Chapter 4. Chapter 5 will present conclusions and suggest future work in the development of ultrasonic temperature measurement technologies.

CHAPTER TWO:

LITERATURE REVIEW

2.1 Introduction

Ultrasonic nondestructive testing has a wide variety of applications in a variety of industries, including medical; structural health monitoring, e.g. [6,7]; damage detection in composites, e.g. [8–10]; temperature measurement, e.g. [11–23], flow monitoring, e.g. [24,25]; and characterization of material nonlinearity, e.g. [26,27].

The noninvasive nature of ultrasound coupled with its relatively low cost compared to other nondestructive evaluation techniques makes it a desirable technique for many applications.

2.2 Material Characterization and Process Monitoring

Ultrasound is often used for materials characterization and process monitoring for quality control purposes (see e.g. [28]). Ultrasound is particularly useful for these purposes because of its ability to test the quality of a part in-situ without inducing damage. The complex nature of materials such as polymer composites requires the development of techniques that can nondestructively test for indicators of quality in manufactured components. When compared to traditional mechanical testing techniques such as bend tests or axial loading tests that destroy a sample part, ultrasonic testing is often a quicker and lower-cost alternative that also maintains the integrity of the part. Thermoset curing, extrusion and injection molding monitoring, and food quality

monitoring are just some of the common uses for ultrasonic testing for materials characterization and process monitoring, and will be discussed in detail below.

2.2.1 Thermoset Curing

Thermosets, a variety of polymers that cross-link to form strong polymeric materials, occupy a sizable area of interest in ultrasonic NDE. Sia *et al.* [29] examined the ability of differential scanning calorimetry (DSC) and dynamic mechanical thermal analysis (DMTA) to monitor loss modulus, a polymer property that changes with degree of cure, and compared these with then-current ultrasound techniques. Sia *et al.* noted that the ultrasound techniques failed to adequately characterize the polymer when cure is above 80%. The conclusion of Sia *et al.* was that DSC and DMTA were useful for determining degree of cure in thermosets, but proposed that an acoustic emission technique be developed to quantify the degree of cure of thermosets with a higher degree of accuracy and confidence in the last stages of cure. Lionetto and Maffezzoli [30–32] have explored the ability to use ultrasound to measure degree of cure in epoxy resins used in fiber-reinforced composites and related applications. Their lab's work has been summarized in a paper presenting two techniques they have developed [31]. One technique uses contact ultrasound in a parallel plate rheometer to monitor speed of sound and attention as a function of cure. Not only were they able to identify gelation and vitrification times, phase transformations during cure, but were able to determine degree of cure more precisely using ultrasound than the standard DSC technique, which could only sense degree of cure to around 75% of full curing. This answered the proposal put forth by Sia *et al.* for a more accurate thermoset cure monitoring technique above 80% cure.

Additionally, a technique was developed to monitor cure using a non-contact ultrasound technique by Lionetto and Maffezzoli [31,32]. This technique produced results similar to the contact ultrasound method as well as the rheological study but for applications outside the rheometer. These similarities showed it to be a reliable method for monitoring changes in the viscoelastic properties at gelation and vitrification.

2.2.1.1 Plastic Extrusions—Filler Content Identification

Ultrasonic testing has also been used for the purpose of determination filler content in composites. Sun *et al.* [33] utilized an artificial neural network (ANN) approach for the determination of filler content in composites. Specifically, an ANN was developed to determine the content of calcium carbonate powder in a polypropylene matrix on the basis of ultrasonic variables. Ultrasonic variables considered were speed of sound and change in attenuation coefficient, and were used in combination with pressure, feed rate, and melt temperature to determine filler content. Moderate success was reported for the use of an ultrasound-focused ANN as a method for filler content determination.

Halmen *et al.* [4] used knowledge of the relationship between speed of sound and filler content of polypropylene (PP) to spatially image radial filler gradients in extruded rods of PP. Using a radon transform and a circular array of 40 ultrasonic transducers, they were able to reconstruct images of these extruded rods. This in-line imaging technique has implications for further development of process control and monitoring of plastic extrusions. Halmen *et al.* notes that there is significant work to be done before this can be reliably used in industry, but demonstrated the feasibility of such a technique.

2.2.1.2 Food Applications

Gregg [2], one of the early researchers of the present work at Baylor University, applied techniques developed for phase monitoring of baking chocolate. Gregg monitored wave speed in baking chocolate as it heated and cooled. Due to the high heat capacity of untempered chocolate, difficulty was encountered with melting the chocolate. However, monitoring of the bulk temperature using ultrasound was found to be accurate to within 1.5 °C based on embedded thermocouple experimental confirmation measurements.

Häupler *et al.* [1] used ultrasonic testing in situ to characterize cocoa butter, the fat phase of chocolate. By monitoring speed of sound and attenuation throughout the crystallization process for cocoa butter, differences could be measured between tempered and untempered cocoa butter. Häupler *et al.* demonstrated the viability of implementation of this technique in industrial chocolate manufacturing. In a later study by the same group, Winkelmeyer *et al.* [3] was able to distinguish between 2, 4, and 6% solid fat content chocolate using similar techniques to Häupler *et al.*

Ultrasonic testing has also been applied to beef roasting quality monitoring. Hæggström and Luukkala [34] monitored speed of sound and attenuation, and measured the nonlinearity of the material to monitor the internal temperature of beef during an automated roasting process. A fitted parametric expression was provided to monitor the internal temperature as a function of speed of sound of the beef.

2.2.2 Temperature Measurement

2.2.2.1 Speed of Sound Temperature Dependency

An early use of sound for the measurement of temperature, the primary focus of this paper, dates back to 1873 [19]. In this study, Mayer used a device which produced

sound in a metal tube. Mayer observed that as the temperature of the air inside the tube changed, the number of wavelengths observed in the tube likewise changed. Mayer's study of the temperature dependency of sound speed would be the start to a broad field of study with applications in a variety of industries.

For example, Chen *et al.* [11] used ultrasonic techniques to monitor polymer extrusions and found that results obtained with speed of sound measurements were in good agreement with thermocouple measurements. Similarly, Takahashi and Ihara [17] used pulse-echo ultrasound to monitor speed of sound within a silicone rubber. Experimental results were compared to a simulation and found to be in good agreement.

Jia *et al*. performed a study for measuring temperatures across gasifier refractories [14]. This was done by crafting a cylindrical cement specimen with structured echogenic features designed to induce multiple ultrasonic reflections that could be captured using a single transducer. By utilizing the echogenic features to measure speed of sound at various depths into the material, they were able to indirectly measure temperature in the material.

In a later study, Jia and Skliar [15] used an experimentally determined speed of sound versus temperature relationship to measure temperature distribution and heat fluxes in cementitious materials using the UltraSound Measurements of Segmental Temperature Distribution (US-MSTD). Measurements performed using the technique from [14] were used to capture temperature distributions. These measurements were compared to a finite element model of the heat distribution in the material geometry and used to experimentally determine heat fluxes as a function of distance in the material.

Schmidt *et al.* [20] used ultrasonic data to measure the temperature inside a large diameter Navy gun barrel. Previously, by measuring the time of flight between two discontinuities in the gun barrel geometry, average sound velocity could be estimated. However, a better temperature measurement method was sought. Schmidt *et al.* developed an inverse method based on the heat conduction equation and simulated data. Once the method was verified using simulated data it was then used experimentally to measure not only surface temperature but predict a thermal profile with heat flux data measured at the rifled surface

Brown *et al.* [5] conducted a study to measure the in-line melt temperature of polymer melts in single screw extruders. By measuring speed of sound values of a polypropylene homopolymer at various temperature and pressure values, knowledge of the pressure-temperature-speed of sound relationship was known. Using this data, ultrasonic sensors were attached in a through transmission configuration to a single screw extruder. By measuring speed of sound during the extrusion process, a bulk temperature measurement was able to be made that was shown to be more accurate than the measurement of surface temperature done using surface thermocouples or infrared sensors. With knowledge of the temperature of the polymer extrusion, process controls can be adjusted for the improvement of the production of the polymer.

2.2.2.2 Temperature Imaging and Reconstruction

Once the basics of the temperature-sound velocity relationship of a material are understood, mathematical algorithms have been implemented to create a 2- or 3-dimensional reconstruction of temperature distributions in a material. For examples, see Liu and Ebbini [16] and Liu *et al.* [18]. Because of the wide use of ultrasound for non-

invasive, internal temperature measurement, much work has been done in the area of creating more efficient and accurate reconstruction algorithms [12,13,16,22,35,23]. Data is typically collected by arranging ultrasonic transducers in a circular or rectangular array around the area of interest. One transducer will send a signal and the signal will be measured on multiple receiving transducers. After many permutations of this are performed, temperature profiles are constructed using a variety of inverse techniques.

The difficulty of temperature reconstruction lies in that it is an inverse problem, meaning that the problem starts with gathering observational data and an attempt is made at determining the physical phenomena that caused this data. In other words, the results are used to determine the causes. Thus, for certain categories of problems, the inverse problem does not have a unique solution. This means that there may exist multiple solutions that may satisfy the results, whereas a physical system can exist in only one of the solutions at any given moment.

The least-squares method (LSM) is one of the most commonly implemented algorithms for solving the temperature reconstruction inverse problem. However, the least-squares method has several limitations. Shen *et al.* [22] presented a new method for temperature reconstruction based on multiquadric interpolation of the least squares method (LSM-MQ). As Shen *et al.* explains, the detail of LSM is limited by the number of paths scanned. Additionally, LSM is restricted from reconstructing data at the edge of the reconstructed area. However, with the new algorithm implemented edge data is reconstructed and, according to Shen *et al.* the reconstruction is more accurate at reconstructing temperature data in a variety of situations. Limitations of the least squares method also include the inability to model phase changes in the material based solely on

speed of sound data. Phase changes, as observed in this study, cause a significant kink in the speed of sound vs. temperature relationship which cannot be characterized using a low order polynomial.

Jia *et al.* [13] likewise improved upon the least-squares reconstruction method. Using the new method, which relies on a radial basis function approximation and singular value decompositions, the well-established relationship between temperature and sound velocity in gases was used to create a two-dimensional reconstruction of a temperature gradient in air. Reconstructions using LSM and the proposed method were compared and the proposed method was found to have a higher overall accuracy in reconstructing the temperature field.

Bramanti *et al.* [23] performed a temperature reconstruction by using an acoustic pyrometer system to obtain thermal imaging measurements in power plant boilers. Using simulated data, this technique was tested and found to be adequate. The presented conclusion was that through the use of more scanning paths, imaging resolution could be drastically improved.

Praher *et al.* [21] demonstrated the feasibility of a temperature reconstruction in two dimensions of polymer extrusions in the screw ante-chamber of an injection molding machine. By inducing beam diffraction using steel buffer rods and ultrasonic transducers arranged in a circular array, Praher *et al.* demonstrated how ultrasound can be used to measure temperature at various angles in order to reconstruct a temperature image using a simultaneous iterative reconstruction technique. This study took into account the relationship between sound velocity, temperature, and pressure to more accurately measure temperature for injection molding improvements.

Through the use of ultrasound, many temperature measurement techniques have been developed for use in a variety of applications. Initially beginning as only the measurement of temperature in materials using ultrasound, the field has developed to create reconstruction algorithms that can image thermal data in a variety of applications with each algorithm having strengths specific to a particular type of temperature distribution or material system. As each of the above-mentioned papers discuss, the strength of ultrasonic inspection for temperature measurement lies in its ability to measure internal temperature of both fluids and solids under extreme temperature or pressure conditions normally impossible or restrictive for normal temperature measurement techniques.

CHAPTER THREE:

ULTRASONIC EXPERIMENTATION

3.1 Introduction to Ultrasonic Theory

Ultrasonic theory is based on the propagation of mechanical acoustic waves in the frequency range typically stated to be lower bounded at 20 kHz. Waves propagate or travel through a medium by creating localized pressure differences within the medium's microstructure, see e.g. [28]. Ultrasonic measurement and propagation is most often done using mechanical transducers, which are based on the use of a piezoelectric crystal and in this research, all ultrasonic transducers used are piezoelectric transducers. Ultrasonic measurement using piezoelectric crystals converts the mechanical energy contained in the vibratory propagation of a wave to an electrical voltage. The voltage created by a piezoelectric crystal is proportional to the mechanical energy contained in the ultrasonic wave. In other words, the intensity of the vibration created in the piezoelectric crystal by the pressure wave is proportional to the voltage output by the transducer. Thus, ultrasonic waves can be monitored and recorded by measuring the voltage drop over an ultrasonic transducer.

An ultrasonic A-scan, the result of a single acoustic pulse into a material and the captured waveform, is a function of the physical state of a material. Ultrasonic A-scans are commonly regarded as the most basic piece of ultrasound data, a typical ultrasonic A-scan from the current work is depicted in Figure 3.1.

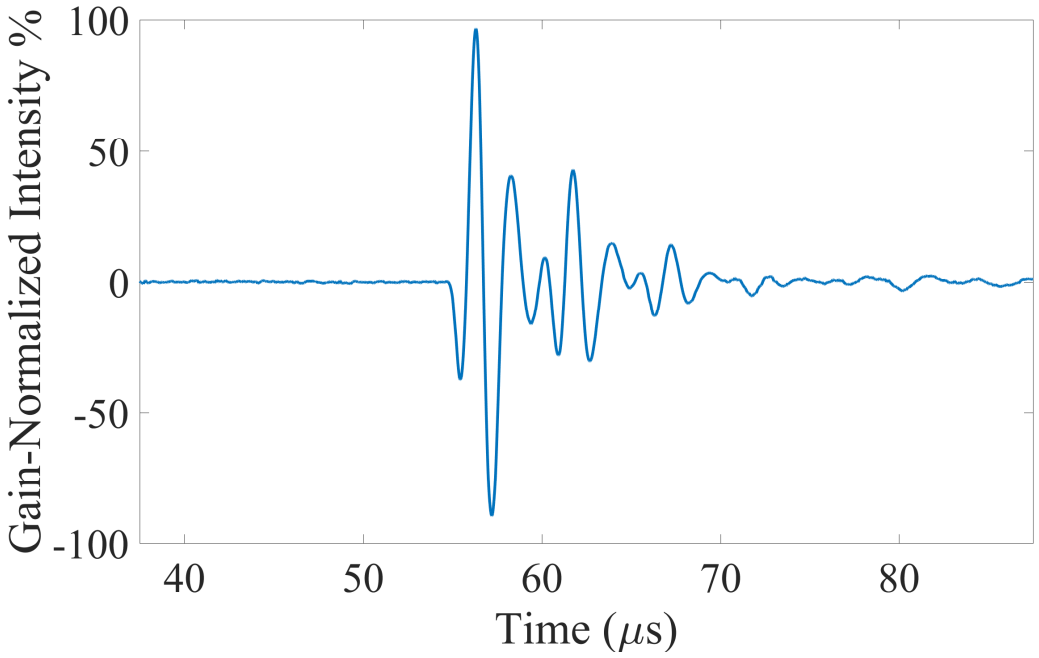

Figure 3.1. Typical ultrasonic A-scan

As Figure 3.1 shows, the intensity of the wave, "Gain-Normalized Intensity" on the y-axis, is captured as a function of time. A pulse width of 20-50 ns was typically used in this work. As can be seen in Figure 3.1, the width of the main pulse, occurring at 55 µs, is approximately 15 µs long. This pulse can be seen to exponentially decay, as evidenced by the general trend of decreasing height of the pulse. Minor pulse reflections can be seen from 70 µs to the end of the scan and are the components of the wave arriving at the receiving transducer slowed down by pores, internal reflections, or discontinuities. The sampling frequency, length of capture time, and other data collection parameters are determined by the data capture device parameters used. Data collection details for the current work will be discussed in Section 3.2.

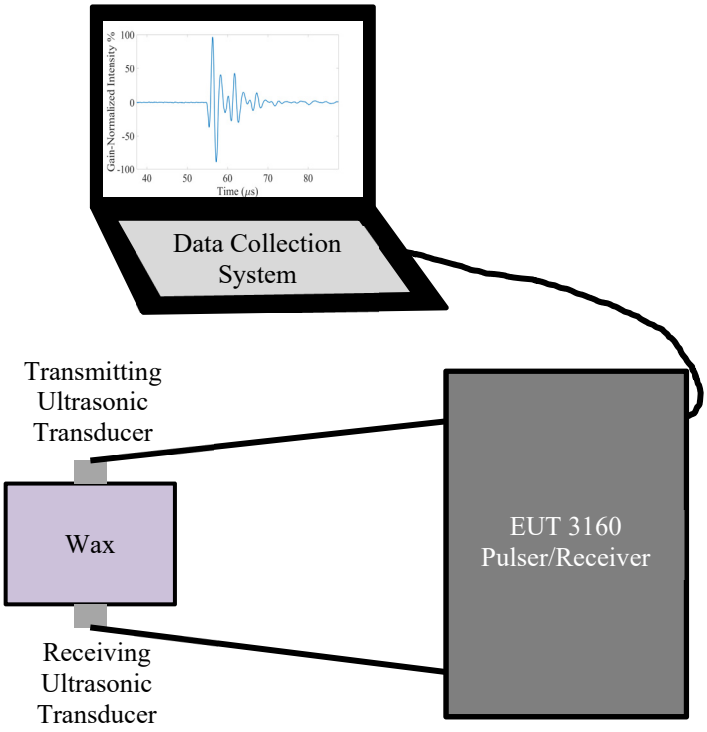

Figure 3.2. Ultrasound Testing Setup

Figure 3.2 shows the ultrasonic experimental setup used to collect data in Figure 3.1. Shown is the specimen, wax; pulser/receiver, EUT 3160; data collection system, laptop; and ultrasonic transducers. In this setup, the EUT 3160 system generates and receives the ultrasonic pulses. The data collection system laptop receives, processes, and analyzes the data sent from the EUT 3160.

3.1.1 Ultrasonic Experimental Configurations

There are three basic ultrasonic experimental configurations: pulse-echo, pitch-catch, and through transmission. The first, pulse-echo, uses a single ultrasonic transducer to both send and receive the ultrasonic wave. An ultrasonic wave is initiated, travels through the medium, reflects off various material changes or boundaries, and travels back to the transducer where it is received and the signal is recorded. A simple way to

understand ultrasonic configurations is to think of the transmitting transducer as a mouth speaking and the receiving transducer as an ear. Thus, in pulse-echo mode, which only uses one transducer, the transducer serves as both the mouth and the ear. Pulse-echo configuration is particularly useful when both sides of a material or part cannot be accessed.

The second configuration, pitch-catch, is similar to pulse-echo, but uses a second transducer to receive the ultrasonic wave. In pitch-catch, the received wave is at an angle not-normal to the reflecting surface. One can imagine pitch-catch mode as speaking to someone around a corner, a situation where the sound reflects off surrounding walls to travel from the speaker to the listener. Like the pulse-echo configuration, pitch-catch is useful for setups which make access to the back of the part difficult or impossible.

Lastly, the through transmission configuration involves placing the transmitting and receiving transducers on opposite sides of the medium of transmission. In this configuration, both sides of the part must be accessible, which limits the potential for applications using this method. However, through transmission was selected as the experimental configuration for the current work because of its simplicity and ease of use as well as ease of access to both sides of the material of interest. Additionally, through transmission is advantageous when compared to pulse-echo because the generated wave does not have to reflect back to the receiver. For example, if a part is 6” thick, the wave captured in pulse echo configuration will have a similar energy to that of a 12” thick part tested in through transmission. This is because the pulse-echo scan receives a reflected wave, which only contains a fraction of the initial wave energy, whereas the through

transmission signal receives a refracted wave, which only occurs at the back wall of the part.

Figure 3.3 presents diagrams of each method of ultrasonic experimental configuration. Transmitting and receiving transducers are indicated with “T” and “R,” respectively. Wave propagation direction is indicated by the red arrows.

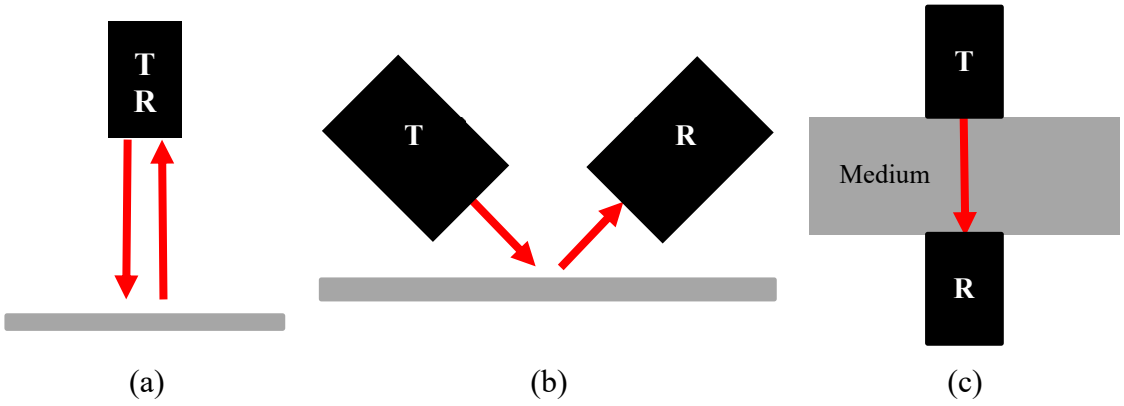

Figure 3.3. Configurations for ultrasonic testing. (a) Pulse-echo, (b) Pitch-catch, (c) Through transmission

3.1.2 Ultrasonic Parameters

One of the most commonly measured parameters using ultrasound is speed of sound. Speed of sound is the bulk velocity at which the ultrasonic wave propagates through a medium. A common method for assessing speed of sound is through a time of flight measurement. Time of flight, or the amount of time a sound wave takes to travel between the transmitting and receiving ultrasonic probes, is used to calculate speed of sound. Time of flight is defined in this research as the moment in time, relative to the initial firing, that the signal intensity of an A-scan exceeds a user-defined threshold saturation percentage. Defining thresholds both below and above the mean signal value is known as the dual-threshold method [36]. In this work, 20% saturation thresholds of the

gain normalized signal, as measured from the mean signal value to the peak signal absolute value, was used to ensure that the signal was being detected as opposed to electrical noise. Speed of sound calculations were performed using an in-house package developed in MATLAB.

Using Equation 1, speed of sound, c, can be easily calculated if time of flight, t_{flight}, and l, the length of the path between transducers, are known. Similarly, path length can be calculated if the speed of sound of the material is known.

$$c = \frac{t_{flight}}{l} \tag{1}$$

Figure 3.4 shows an ultrasonic A-scan used to calculate the speed of sound of a material. In this case, the material being tested was wax. Ultrasonic probes were attached to opposite sides of an 8.5 cm wide box of wax and acoustically coupled using commercially-available ultrasonic gel. Thus, speed of sound was being measured in through transmission mode, as in Figure 3.3 (c). The time of flight was identified as 54 μs from the ultrasonic A-scan shown in Figure 3.4. Because the thickness of the wax is known, speed of sound was able to be calculated using Equation 11 as 1574 m/s.

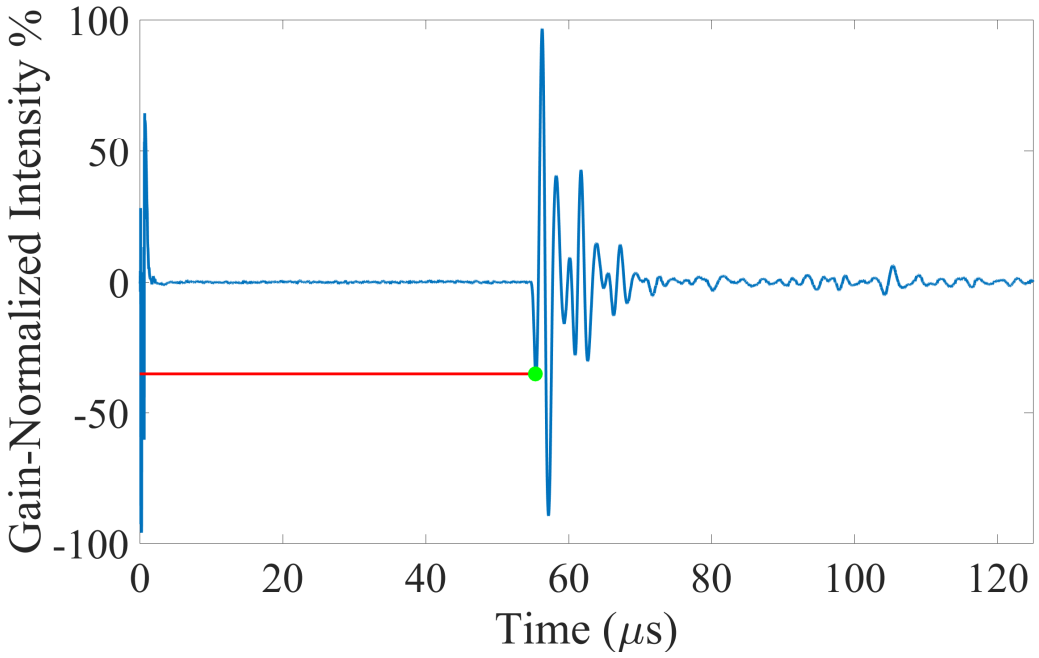

Figure 3.4. A-scan used to measure speed of sound with time of flight marked by red line and green dot.

An additional parameter commonly measured using ultrasound is acoustic attenuation. Acoustic attenuation is a measurement of the energy dissipation, absorption, and ultrasonic scattering in the tested material. Attenuation can be modeled by [28]

$$A = A_0 e^{-\alpha(f)z} \tag{21}$$

where $\alpha(f)$ is a frequency-dependent attenuation coefficient, z is the distance traveled, and A_0 is the initial amplitude of the wave.

Attenuation and scattering of an ultrasonic signal in a material are related to the micro-structure of the material. For example, a very smooth, continuous material such as steel tends to have a low attenuation factor, whereas the materials under investigation in this study are highly-attenuative, due in part to their porosity. Porosity introduces attenuation because the wave is significantly scattered as it travels through the holes in

the material. Because of signal attenuation, the signal must be amplified to capture the signal waveform when it arrives at the receiving transducer. This process will be discussed more in the Section 3.2. Although attenuation is never directly measured in this study, the understanding of this concept is integral to the understanding of this work and the need for gain variations during the change of the internal temperature state.

3.2 Data Collection

Data collection in this study was automated using LabVIEW, a software that allows for the graphical programming of experimental instrumentation. A custom, in-house program was created by the author using LabVIEW to aid in experimentation, data collection, and data processing. This program has two main purposes: 1) automate the data collection process and 2) automate the gain amplification adjustment process.

3.2.1 Automation of Data Collection

The created user interface shown in Figure 3.5 allows the user to set all parameters for the experiment, including low- and high-pass filters, buffer length, sampling frequency, and more. The program provides the user with the ability to choose the save location for test data. Additional test parameters can be set by the user including length of test, scanning frequency, saving frequency, number of A-scans averaged, and other test protocol details. The customizability of the LabVIEW program is the biggest advantage of the program in that it allows the user a wide variety of parameter options suitable for many different testing situations. Using this program, the user can set up an experiment in only a few minutes and allow the program to automate the rest of the process. The testing in this research is often up to 12 hours in length. This has resulted in

convenience for the researchers working on this project as well as an improved quality of the captured data, as will be seen in Section 3.2.2.

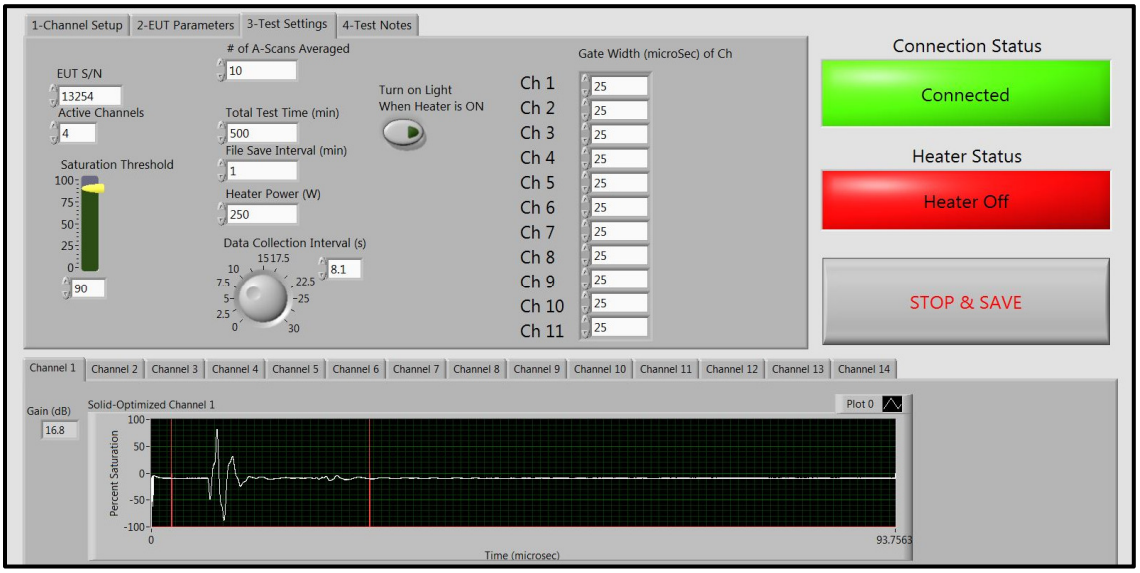

Figure 3.5. Data Collection Program User Interface

3.2.2 Gain Automation

Electrical gain amplification is the increase of the power or amplitude of an electrical signal similar to that of turning the volume knob on a music player. This is done using operational amplifiers and other electrical equipment. For ultrasound, electrical gain, commonly referred to as simply “gain” is a property one can take advantage of to improve results for post-processing procedures and techniques. The system being used has 12-bit data resolution, meaning that there are 2^{12} or 4096 data bins. The gain automation algorithm attempts to keep a gain that will fill a high number of these bins without saturating the signal, to maximize the available resolution.

Electrical gain is defined by comparing the voltage of a signal before and after amplification and is given by (see e.g. [28]).

$$Gain(dB) = 20\log_{10}(\frac{V_{output}}{V_{input}})dB \tag{3}$$

where V_{input} is the pre-amplification voltage and V_{output} is the voltage after amplification. Furthermore, electrical gain amplifies noise, the random fluctuation in an electrical signal [37]. Hardware signal filtering such as low- and high-pass filters and post-processing techniques can be used to increase the signal-to-noise ratio (SNR). SNR is a parameter used to indicate the noise present in a waveform relative to the signal. A high SNR is desired because this means the potential for noise to interfere with signal clarity is diminished. Examples of both low and high SNR signals are shown in, respectively, Figure 3.6 and Figure 3.7.

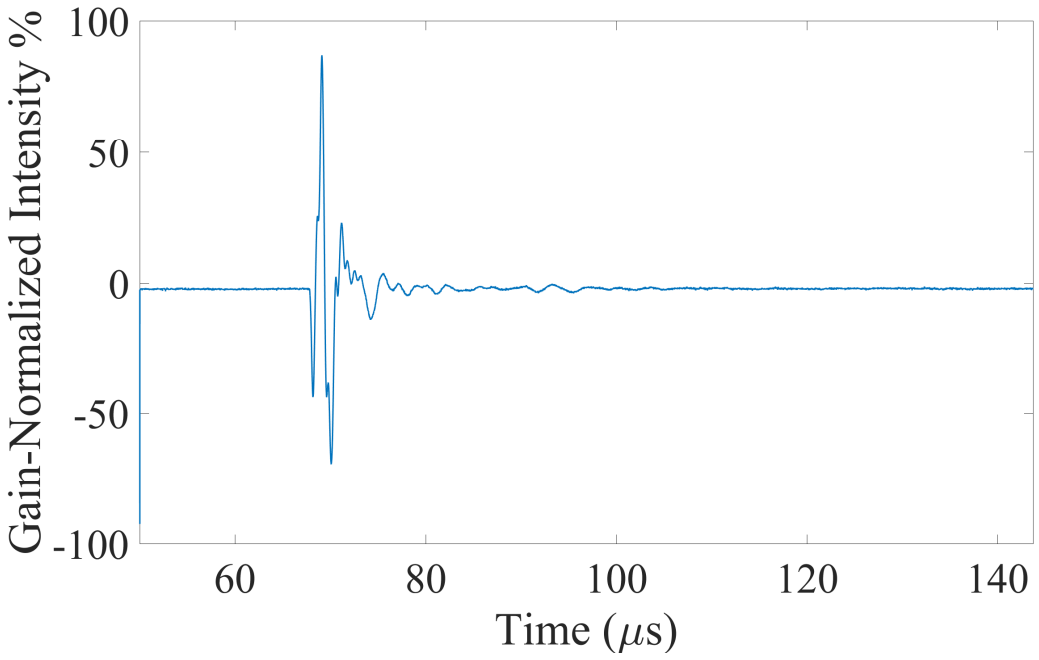

Figure 3.6 Example of a Low SNR Signal

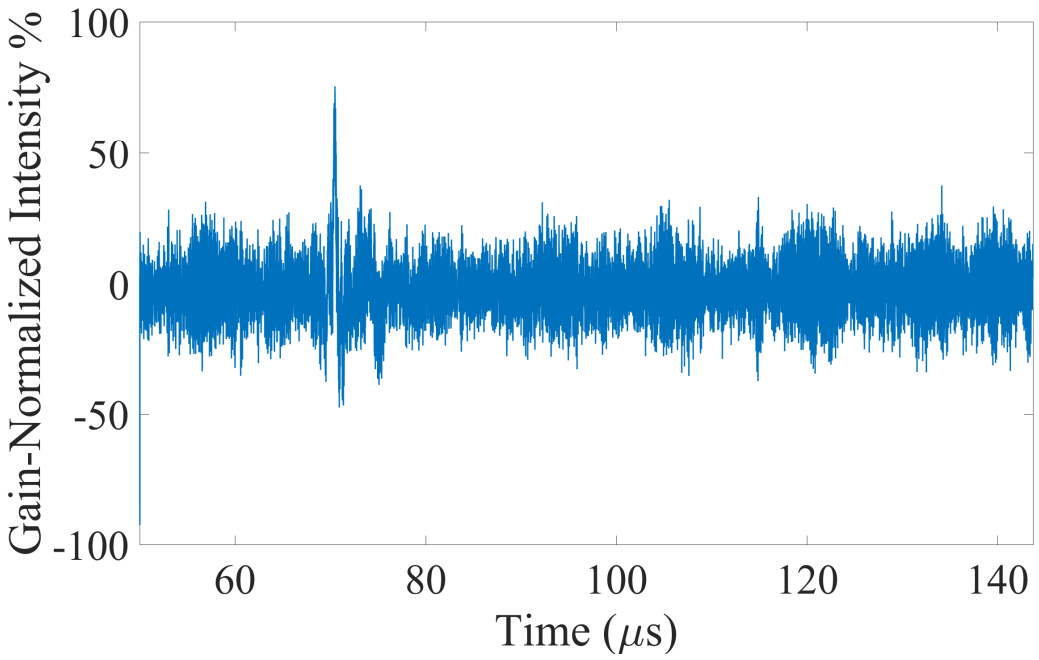

Figure 3.7 Example of a High SNR Signal

Throughout the heating and cooling experiment, the necessary electrical gain to achieve a desired signal saturation changes drastically. This necessitates a program which is able to quickly determine the proper gain, then capture and save the ultrasonic signals. The created LabVIEW program was written by the author to automatically adjust the electrical gain to acquire the highest available resolution signal. First, the user inputs a desired threshold, or the maximum saturation of the signal. Next, while the experiment is running, the LabVIEW program will, using Equation 3, determine the appropriate electrical gain amplification for the signal at that point in time. Then, the program will save the ultrasonic signal with the appropriate gain and repeat the process on the next acoustic path.

Automated gain amplification effects are shown in Figure 3.8, Figure 3.9, and Figure 3.10. The desired maximum signal amplitude is shown at 95% in these figures and indicated by the dashed red line. If the gain of the signal is too low, as in Figure 3.8, the signal will have a poor clarity. If the gain is too high, as in Figure 3.9, the signal will contain clipping, in which the amplitude of the signal exceeds the maximum measurable value. Clipping results in an inability to properly perform mathematical post-processing. If the gain of a signal is set properly, the signal will have a high data resolution without experiencing clipping or over-saturation, as shown in Figure 3.10.

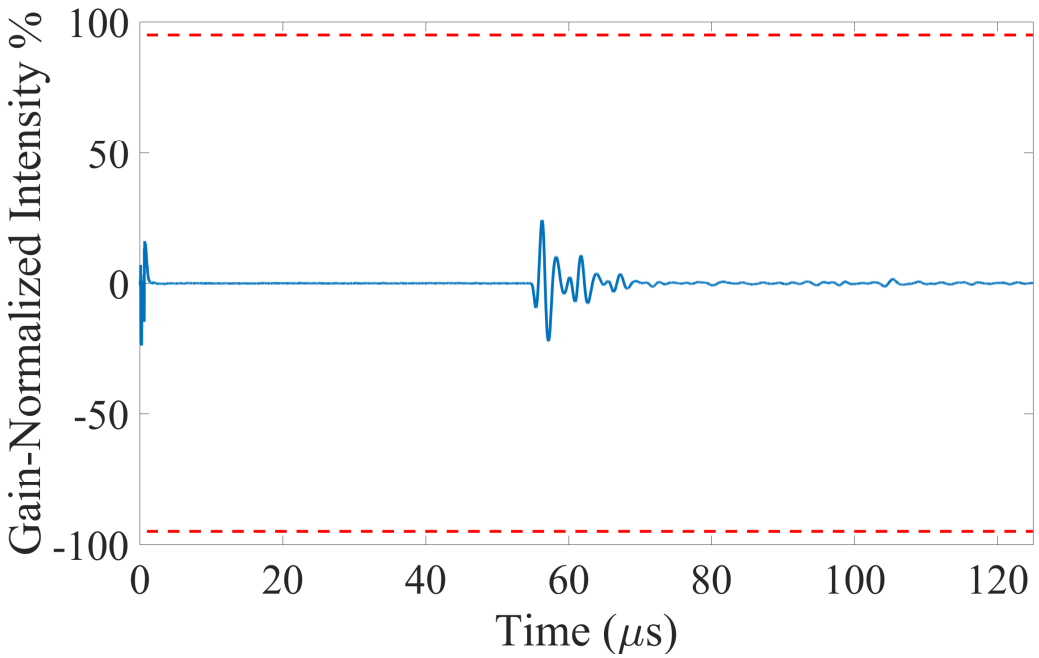

Figure 3.8. A-scans with gain too low.

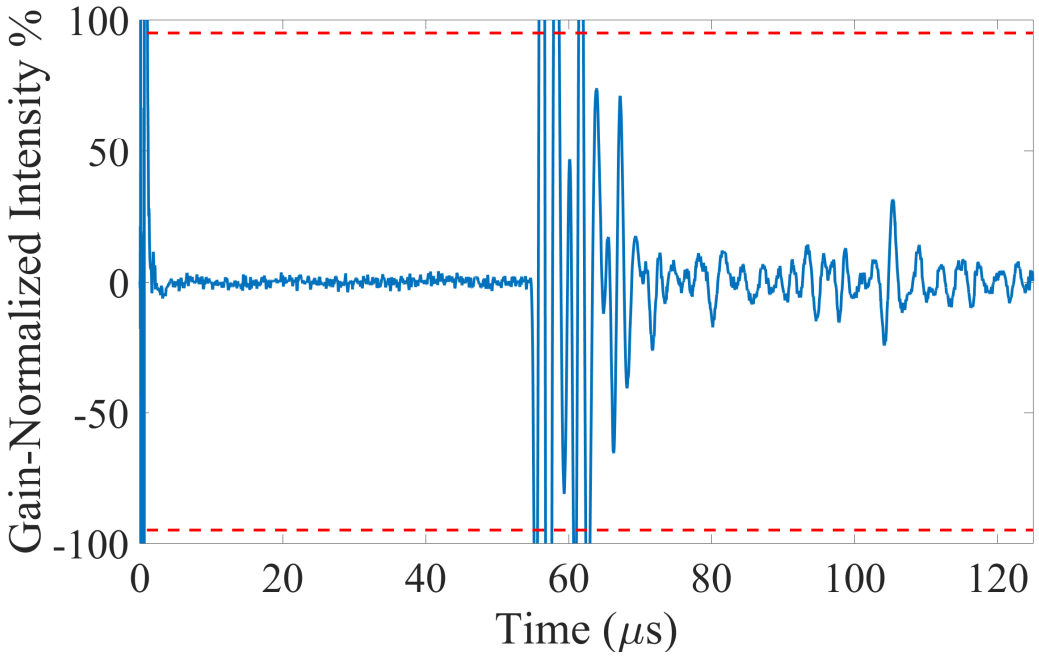

Figure 3.9. A-scan with gain too high.

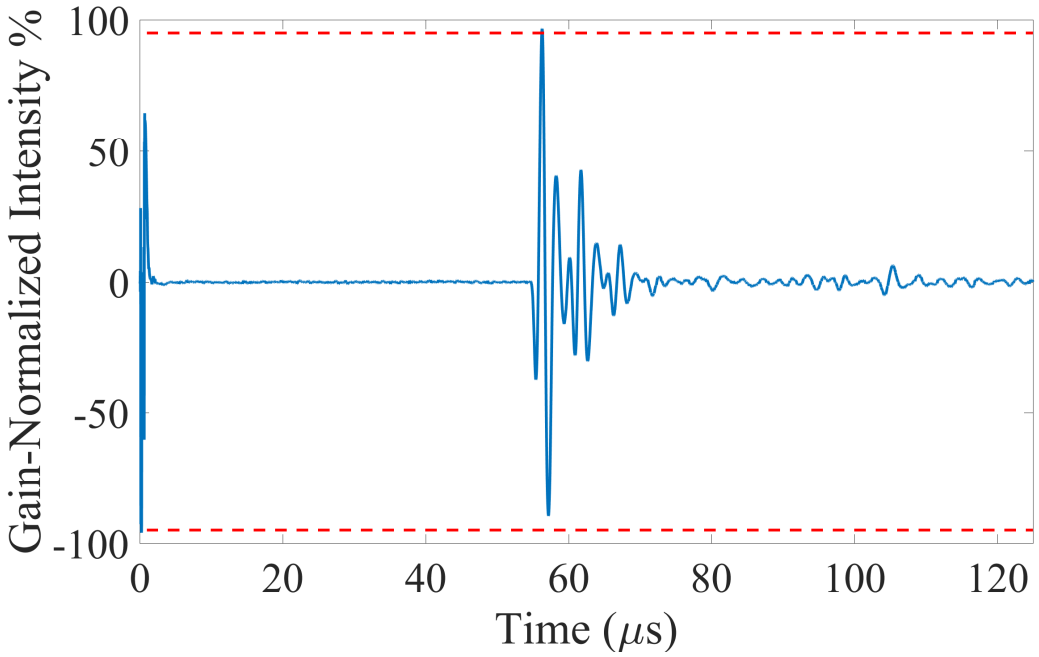

Figure 3.10. A-scan with proper gain.

The appropriate electrical gain is a function of the attenuation factor of the material and the distance the wave travels within the material because the signal will need to be amplified more if it is weak when it is received. As results presented later will show, the appropriate electrical gain to achieve a desired maximum signal saturation is strongly correlated to the temperature and phase of the tested material. This correlation will be taken advantage of in Chapter 4 in order to infer the material phase and internal temperature state of a material.

3.3 Experimental Setup

3.3.1 Experimental Equipment

The experimental equipment chosen for this study was required to have multiple channel capability, programmable capability, and be able to produce a high-energy ultrasonic signal. The selected pulser/receiver, the device that creates and receives the ultrasonic pulses used in this research, is the US Ultratek EUT 3160M8 pulser/receiver, shown in Figure 3.11. This device has 16-channel capability, can be programmed using LabVIEW, is portable, and has a wide variety of settings that allow for future improvement of experimentation and data collection. The EUT3160M8 has a maximum sampling frequency of 160 MHz, gain amplification range of 0-80 dB, and is capable of operating in all three ultrasonic configurations, as detailed in the Section 3.1.1.

Figure 3.11. US Ultratek EUT3160M8 16-Channel Pulser/Receiver

Olympus 0.5 MHz, 1.0 in. Videoscan flat face circular transducers were chosen as the transducers for this study. These transducers are able to create the high-energy ultrasonic pulse necessary to travel through the high-attenuative materials being tested in this study. Pictures of a transducer are shown in Figure 3.12.

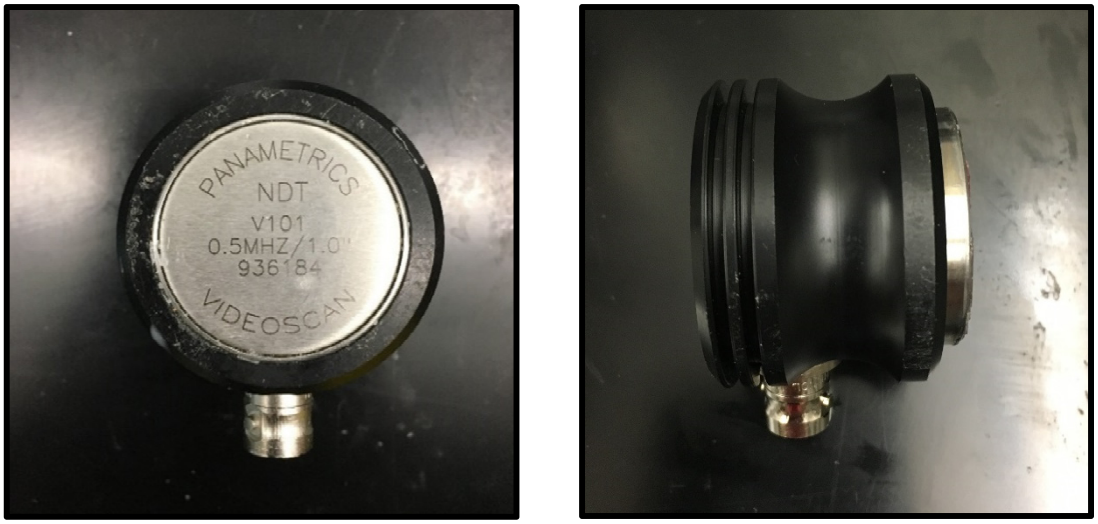

(a) (b)

Figure 3.12. Olympus Transducer (a) Front View (b) Side View

For temperature data acquisition, a Graphtec GL820 Data Acquisition device was selected. This device offers expanded configurations allowing for the measurement of temperature using many thermocouples, and in the present work as many as 29 thermocouples were used in any given test. The Graphtec GL820 is shown in Figure 3.13. Watlow K-type thermocouples were selected for use because of their precision in the temperature ranges being tested. The thermocouple type used is shown in Figure 3.14.

Figure 3.13. Graphtec GL820 Data Acquisition Device

Figure 3.14. Watlow K-Type Thermocouple

A Watlow Firerod heating element was used to melt the wax. A picture of the heating element and the 6.3 cm x 6.7 cm x 2.5 cm aluminum block it was embedded in is shown in Figure 3.15. This heating element was controlled by a heater box, shown in Figure 3.16.

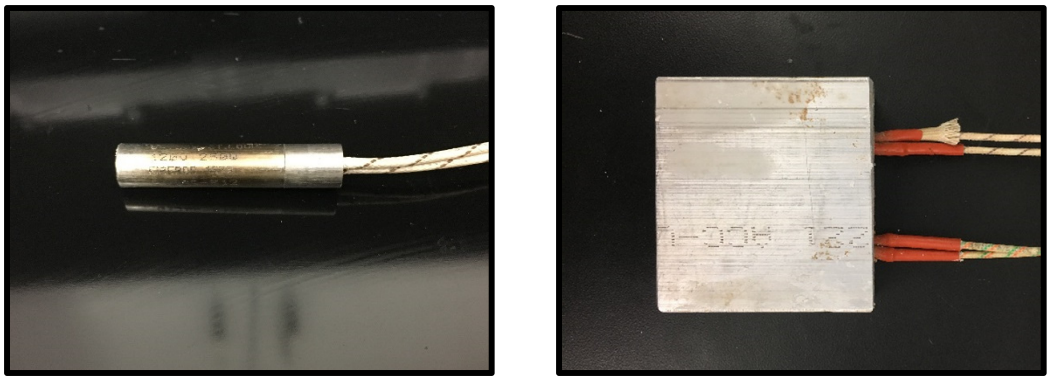

(a) (b)

Figure 3.15. (a) Watlow Heating Element (b) Aluminum Heating Block

Figure 3.16. Heating Element Controller

3.3.1.1 Apparatus Selection

Because the purpose of this work is to non-invasively measure phase changes and monitor internal temperature of highly-attenuative materials, an experimental setup was developed that would allow for materials to be studied in multiple material states. The experimental setup involves an open-top acrylic box with a wall thickness of 0.63 cm and inner dimensions (L x W x D) of 20 cm x 8.5 cm x 15 cm. Acrylic was selected because it is a clear polymer with a high melting temperature. Using custom mounts, four transducers were attached to the side of the acrylic box and acoustically coupled using Sonotech II Gel, a commercially-available acoustic gel couplant. Transducers on one side of the box were set to transmit an ultrasonic pulse to be received by transducers on the opposing side of the box. It has been shown in a related study [2] that for the purposes of this work neither the direction of through transmission nor the temperature changes in acrylic affect results.

A 6.5 cm x 6.5 cm x 2.5 cm aluminum block containing a controllable heating element was immersed in the material of interest on one end of the box. Thermocouples were inserted vertically in the material to measure the temperature of the material throughout the experiment. By having the heater block at one side of the box, the material melted from one side of the box to the other. This setup was selected because it allows for through transmission ultrasound, visual confirmation of material state, and possessed a simple geometry. Several sizes of apparatus were constructed, however diagrams of the apparatus used in the majority of the presented results are presented in Figure 3.17 and Figure 3.18. A picture of the setup is shown in Figure 3.19.

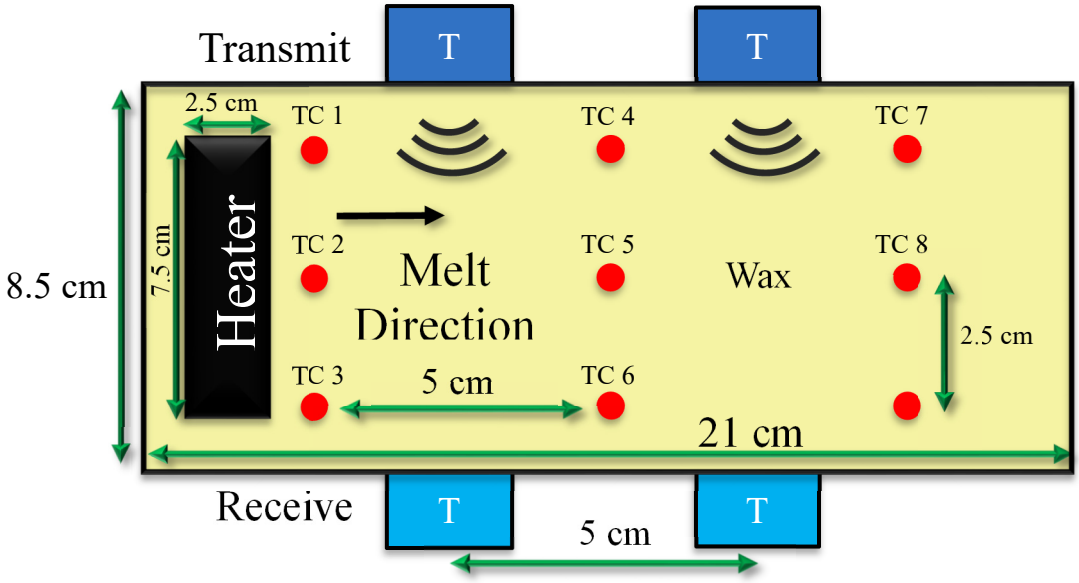

Figure 3.17. Top-View Diagram of Rectangular Experimental Apparatus

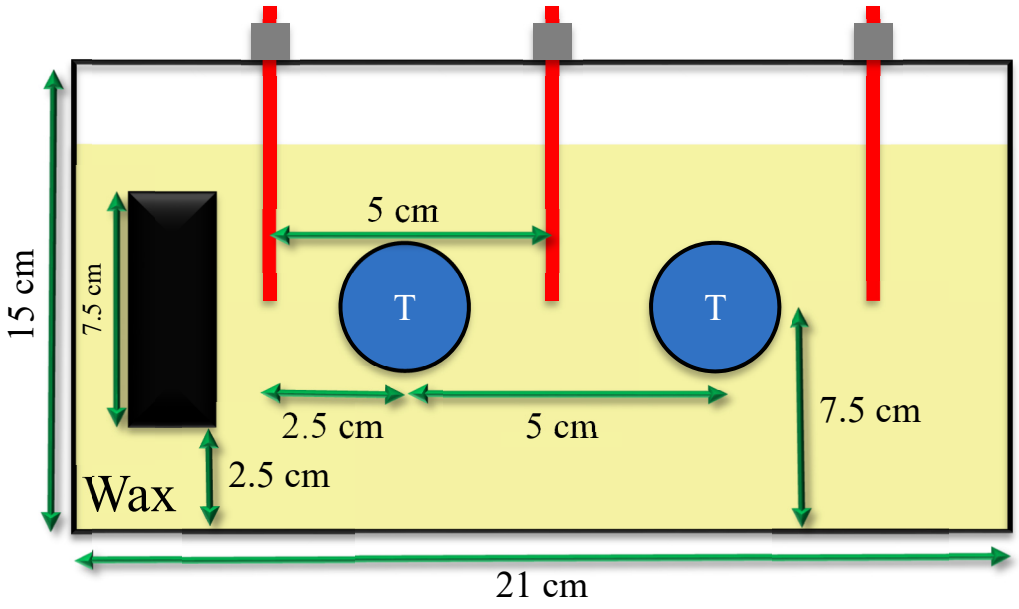

Figure 3.18. Side-View Diagram of Rectangular Experimental Apparatus

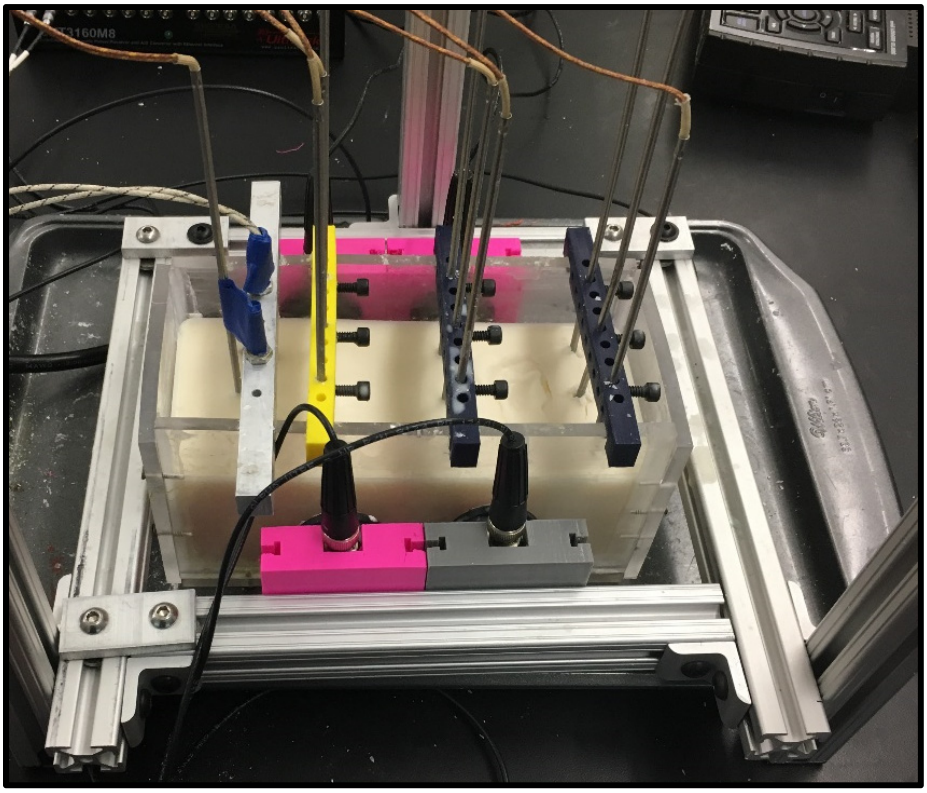

Figure 3.19. Picture of Rectangular Experimental Apparatus

In addition to the rectangular experimental apparatus, a cylindrical geometry apparatus was used for testing, as depicted in Figure 3.20. Unlike the rectangular apparatus, in which the melt direction is perpendicular to the scanning direction, the circular geometry with a centered heating source has the melt direction always approaching each transducer normal to the face of the transducer. In other words, the melt front and the ring of transducers form concentric circles. By observing the melt direction in a different way, the robustness of determined temperature and phase measurement techniques can be tested.

The circular geometry apparatus was constructed using an aluminum paint bucket. Similar to the rectangular geometry apparatus, a Watlow heating element was embedded

in a cylindrical aluminum block which was immersed in the wax. The aluminum heating block was suspended in the radial center of the bucket so that radial symmetry could reasonably be assumed. Figure 3.20 shows a diagram of the cylindrical geometry setup. Thermocouples inserted down to the level of the transducers, 25 cm, in the 35 cm deep bucket are shown in order from TC 1 to TC 9.

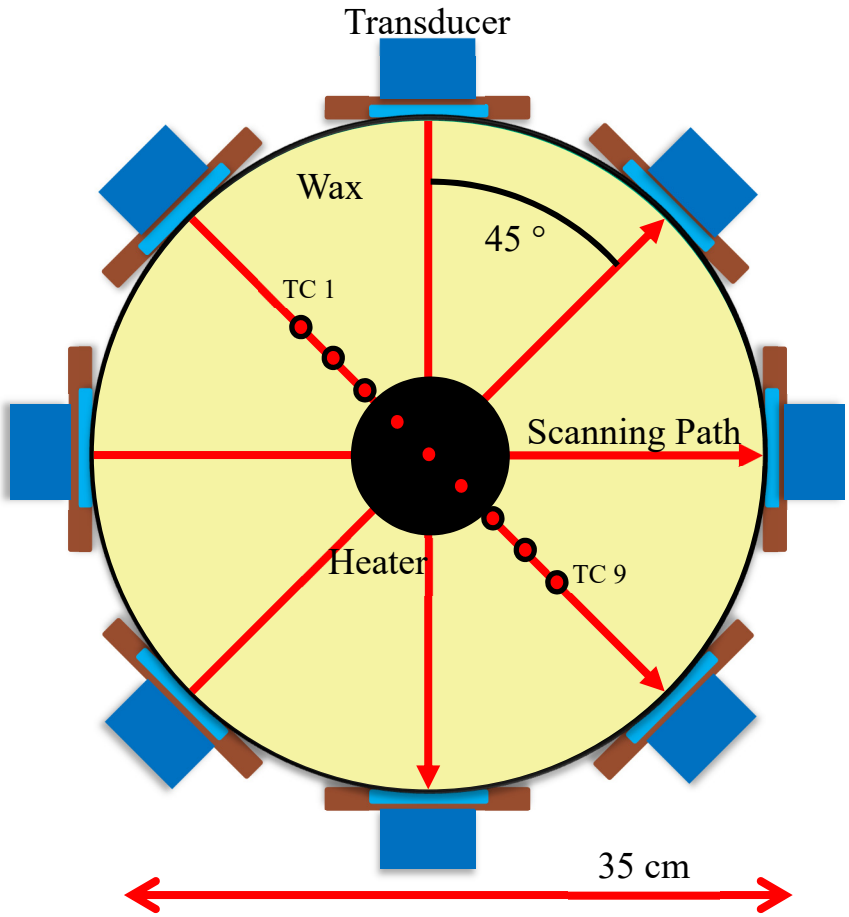

Figure 3.20. Cylindrical Geometry Diagram.

Thermocouples were inserted into the wax in an axially symmetric pattern and only employed a line of thermocouples that crossed through the center of the wax, as

shown in Figure 3.20. Because the wax was only to be melted from the center and thus create an axially symmetric heating pattern this was a determined to be a valid assumption. A picture of the cylindrical geometry setup without the thermocouples is shown in Figure 3.21.

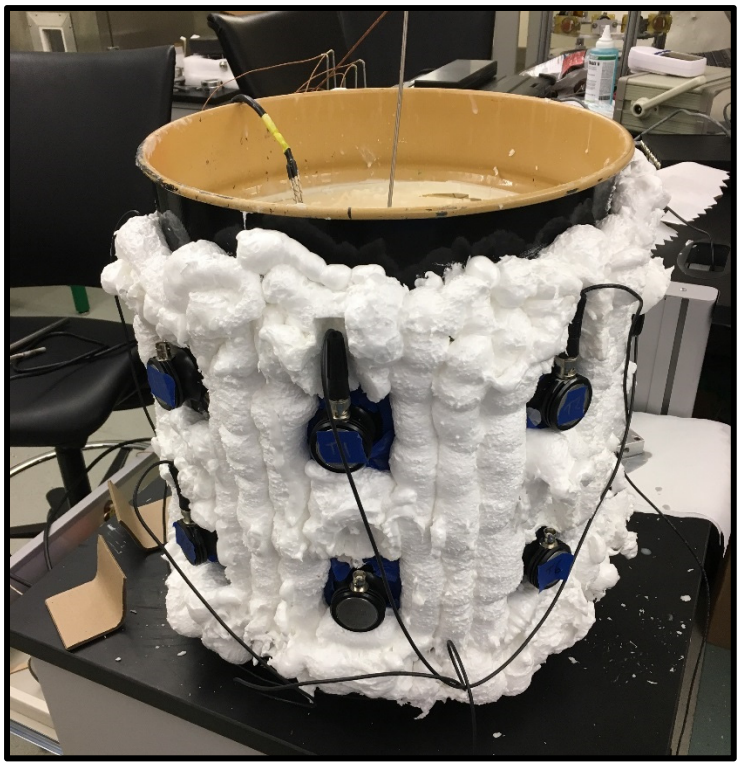

Figure 3.21. Cylindrical Geometry Experimental Apparatus

CHAPTER FOUR:

EXPERIMENTAL RESULTS

4.1 Material Selection and Characterization

For this study, we sought a material was needed that would exhibit multiple phases within an attainable temperature range, was amorphous or semi-crystalline, meaning it has little or no regular molecular rigidity, and would change phases over a range of temperatures. These characteristics were desirable because one of the objective applications is characterizing a thermoplastic near its melt temperature. EcoSoya wax was chosen because it matched these criteria. EcoSoya, unlike many other materials such as water, transitions phases over a range of temperatures, similar to that of a thermoplastic as it transitions to a melt. Conversely, many other materials such as water transition between liquid and solid at a precise temperature value. This phase transition property of the material of interest presents a unique challenge for detecting phase changes in the material; namely, a semi-crystalline material has a range of temperatures it will undergo as the material goes from a solid-like state to a liquid-like state. Differential Scanning Calorimetry was used as an established technique to help quantify the phase change over a range of temperatures in the EcoSoya wax.

4.1.1 EcoSoya Wax

EcoSoya Pillar Blend Wax, a soy-based wax typically used in candles, was selected as the primary test material for this study because of its low melting temperature, non-hazardous characteristics, and likeness to other amorphous and semi-crystalline

materials of interest. To answer the question of how to define a phase change in a material that changes phases over a range of temperatures, Differential Scanning Calorimetry (DSC) was used. DSC is an in-laboratory technique conducted on a small sample, typically 5-8 mg, that measures heat flow of a material sample as a function of material temperature. This is accomplished by comparing temperatures of a material sample and a reference as they are exposed to heat.

Figure 4.1 shows the results of a typical DSC test from a TA Instruments Q20 Differential Scanning Calorimeter for the EcoSoya Wax. The results in Figure 4.1 are from a test conducted on a 5.312 mg sample of EcoSoya Pillar Blend Wax with a heat rate of 2 °C/min. The mass of the sample was obtained using the sub-microgram resolution balance of a TA Instruments Q50 Thermogravimetric Analyzer (TGA). As Figure 4.1 shows, the EcoSoya Wax used in this work experiences full melt at 54 °C as it is heated and a full solidification at 48 °C as it cools. These numbers were identified by finding the maximum and minimum heat flow values in the first cool down and the second heat and their corresponding temperatures using MATLAB. The sample was heated, cooled, heated again. This procedure was used because it is the standard technique for testing thermoplastics, another semi-crystalline material, developed to form a known cooling rate of the material. For many semi-crystalline materials, the degree of crystallinity affects the melt temperature, and the degree of crystallinity is a function of the cooling rate while the material solidifies.

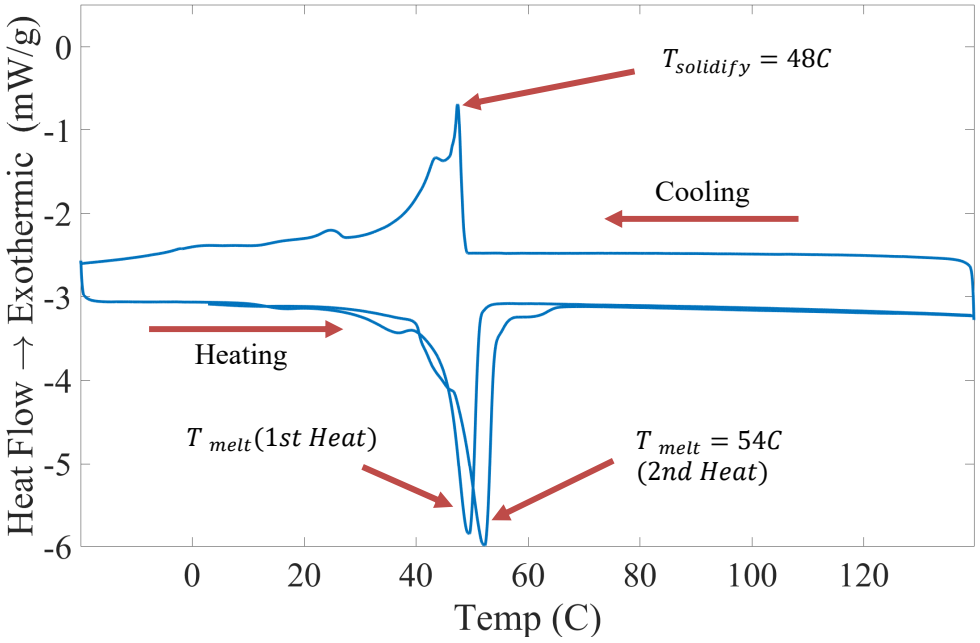

Figure 4.1. EcoSoya Wax DSC Results

It is important to note that due to the nature of the material changing phases over a range of temperature values, the aforementioned temperatures are the complete melt and solidification temperatures for the specific heating rate of 2 °C/min used in the above DSC experiment. In other words, melt or solidification is occurring within a range of temperatures containing the mentioned temperatures. Additionally, the heat rate of DSC testing can have an effect on the measured complete phase change temperatures [10]. Thus, phase changes, as shown by the valley shape in the data between approximately 40 °C and 55 °C in Figure 4.1, occur in EcoSoya wax within a several degree range on both sides of these temperatures. Interestingly, the obtained DSC results for EcoSoya Wax reveal characteristics similar to that of thermoplastic polymers [38], which also have a melt transition over a range of temperatures. The curve in Figure 4.1 during the heating

portion looks very similar to that of a thermoplastic as it is heated through its melt transition.

4.2 Experimental Procedure

4.2.1 Rectangular Geometry Procedure

In order to melt the wax, the heating element was kept at a constant temperature between 175 °C and 250 °C, depending on desired melt rate. Tests were performed at various heating element temperatures to test the effects of melt rate on the effectiveness of temperature and phase change detection. For the tests conducted with a heater temperature of 210 °C, the wax melted over a period of approximately 2 hours. The wax melted with a distinct melt front boundary between liquid on the left and solid wax on the right, as shown in Figure 4.2. The heating temperature was kept constant until the entire box of wax was melted across both transducers, and there was little change in the measured temperature state, at which point the heating element was turned off. The wax was then allowed to cool to room temperature by way of convection while data continued to be collected. Because the box had an open top and the acrylic walls serve as an insulator, the wax was cooled in a horizontally uniform pattern from the top down.

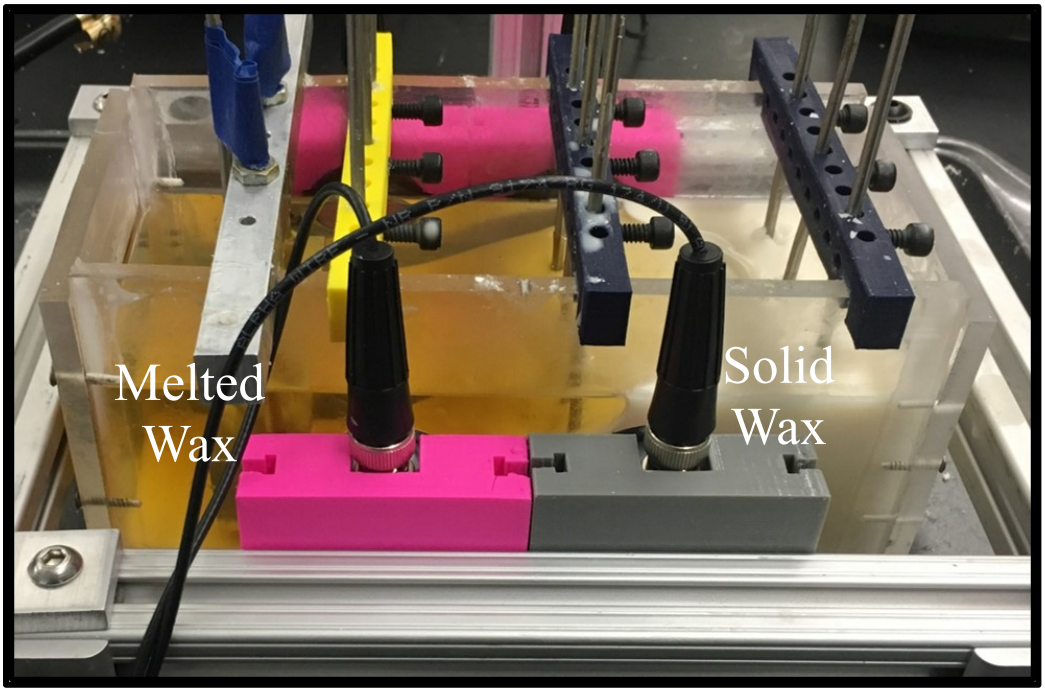

Figure 4.2. Wax Melting with visible melt front (melted wax, left; solid wax, right)

Throughout the entire heating and cooling process, thermocouples inserted vertically into the wax captured the temperature of the wax at the specific locations shown in Figure 3.17. Thermocouples were arranged in rows between the transducer paths to avoid interference with the ultrasonic wave signal. The purpose of the thermocouples was to log the temperature, which were used later to validate the temperature measurements inferred by analysis of the acoustic signal.

Figure 4.3 presents internal wax temperature measured by thermocouples as a function of experimental time for a typical test. The temperature of the wax increases rapidly at the beginning of the test as the heater stabilizes at its set temperature and the wax near the heater block melts. As more thermal energy is applied to the system from the heater, the wax melts completely. At 110 min, marked by event (i) the heater is shut off and the temperature in the entire box decreases. A clear kink in the curve can be

identified at approximately 150 min into this test, marked by event (ii). This will later be shown to be the liquid to solid phase change. Heat capacity, the amount of heat required to change a material's temperature, can be directly measured from the slope of the DSC data, shown in Figure 4.1. Similarly, the kink in Figure 4.3 is indicative of a change in the cooling rate with respect to time of the EcoSoya wax. In this way, the kink can be used to identify phase changes. The lesser slope after this kink demonstrates the slower cooling rate of the wax while in a solid state—a physical manifestation of the lower heat capacity of solid wax when compared to liquid wax.

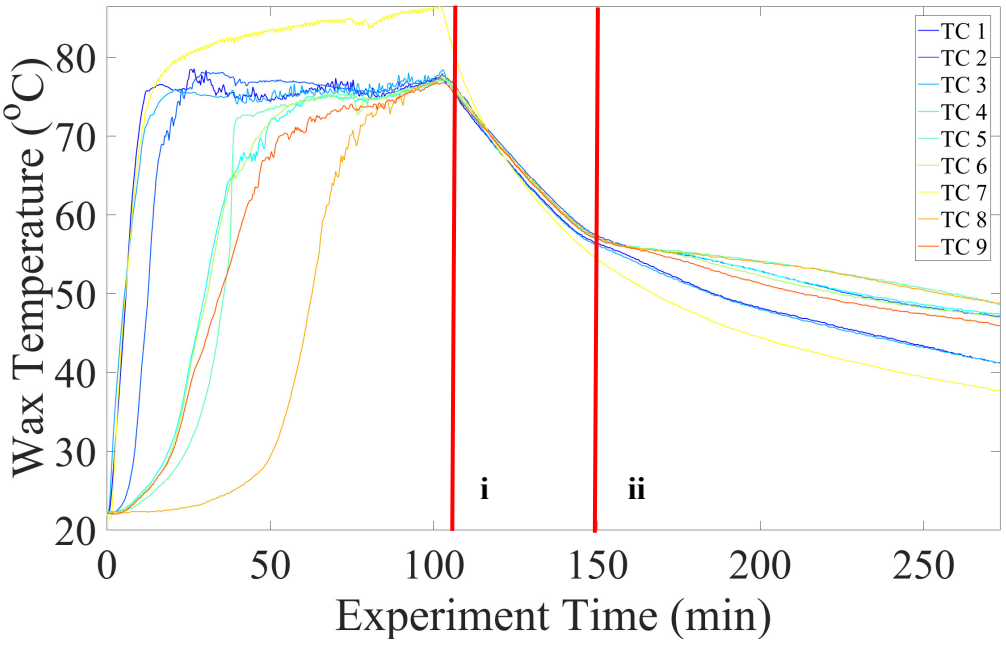

Figure 4.3. EcoSoya Temperature Chart

4.3 Data Processing

All ultrasonic data was collected using the custom LabVIEW program previously discussed. Data was then imported into a custom MATLAB script. The collected raw

ultrasonic data is first de-noised using a discrete wavelet transform. Then wavelet decomposition, coefficient thresholding, and wavelet reconstruction are performed in succession. This de-noising technique allows for a clearer visualization of the data for improved post-processing of the results.

The advantage of de-noising signals using a discrete wavelet transform can be seen in Figure 4.4. This figure shows a noisy ultrasonic signal collected during a test as well as the same signal after de-noising has been performed.

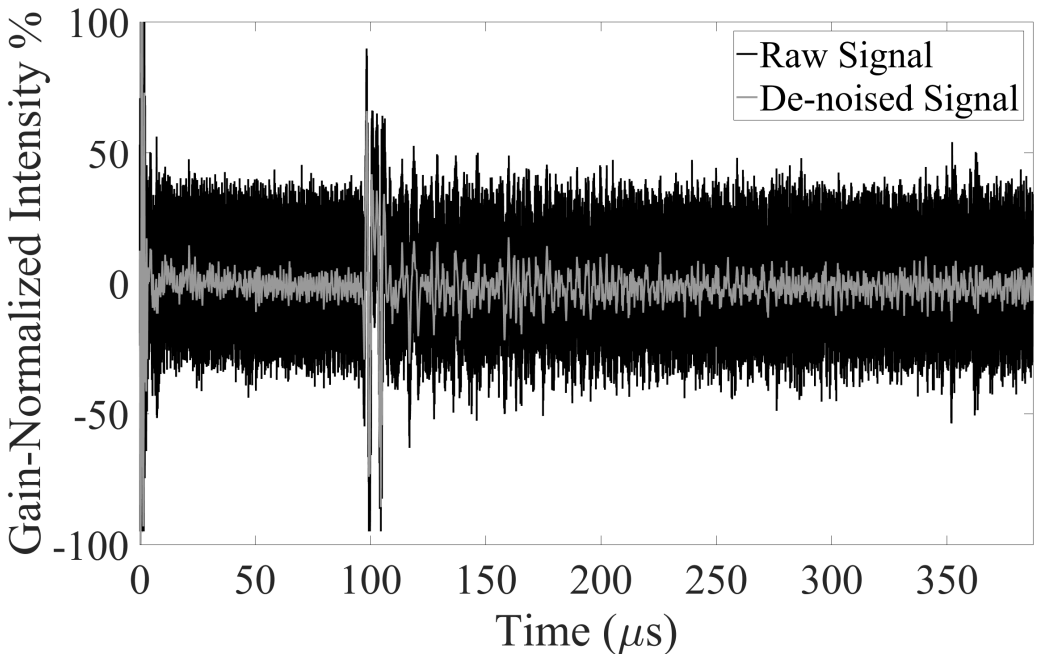

Figure 4.4. A-scan after discrete wavelet transform de-noising

4.3.1 Phase Change Identification

Phase change identification was an important focus of this study. Ultimately, four phase change identification techniques were identified for use in the rectangular geometry scenario where the melt front direction is perpendicular to the ultrasonic scanning direction. The four methods of identification are: the shape of the A-scan, speed of sound monitoring, gain monitoring at signal saturation, and frequency decomposition.

4.3.1.1 A-scan Shape

During the course of experimentation, it was discovered that the shape of the collected ultrasonic waveform, or A-scan, can be used for inferring the phase of the material in the rectangular geometry setup. Figure 4.5, Figure 4.6, and Figure 4.7 show the pattern exhibited in the ultrasonic A-scans collected during a material heating and cooling process in the present study. As a general rule, a direct correlation can be seen between the number of distinct signals in an A-scan and the number of distinct phases across the face of a transducer. For example, Figure 4.5 shows one signal appearing at 55 μs during the portion of the test that the material system analyzed is fully solid. When the transducer face is covered by a distinct solid/liquid boundary as in Figure 4.6, two distinct signals are observed. The first signal, at 55 μs, will be referred to as the "solid signal" and the second, at 70 μs, as the "liquid signal". The time separation between the solid and liquid signals is due to discrepancies between the longitudinal bulk velocities of the ultrasonic signal in the solid and liquid material. In other words, the wave travels faster in the solid wax, arriving at 55 μs, while the wave traveling in the relatively slow liquid wax, does not arrive until 70 μs. Figure 4.7 shows an A-scan when the transducer

face is completely covered by the liquid signal. Because there is no solid wax in the acoustic path of the transducers, the solid signal has disappeared on the A-scan.

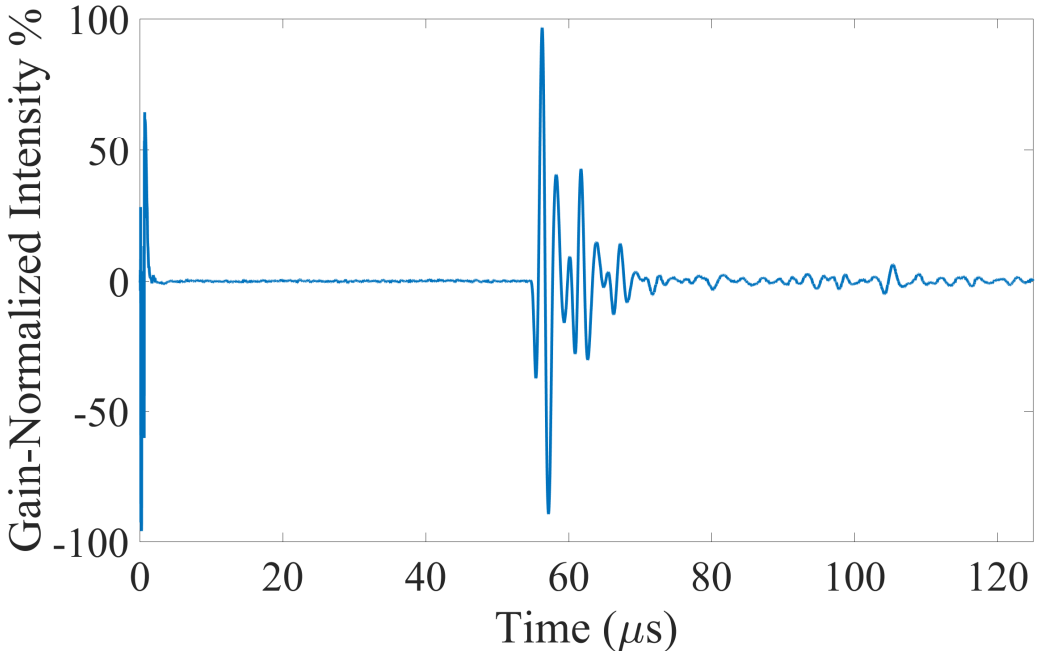

Figure 4.5. A-scan with solid material covering entire transducer face

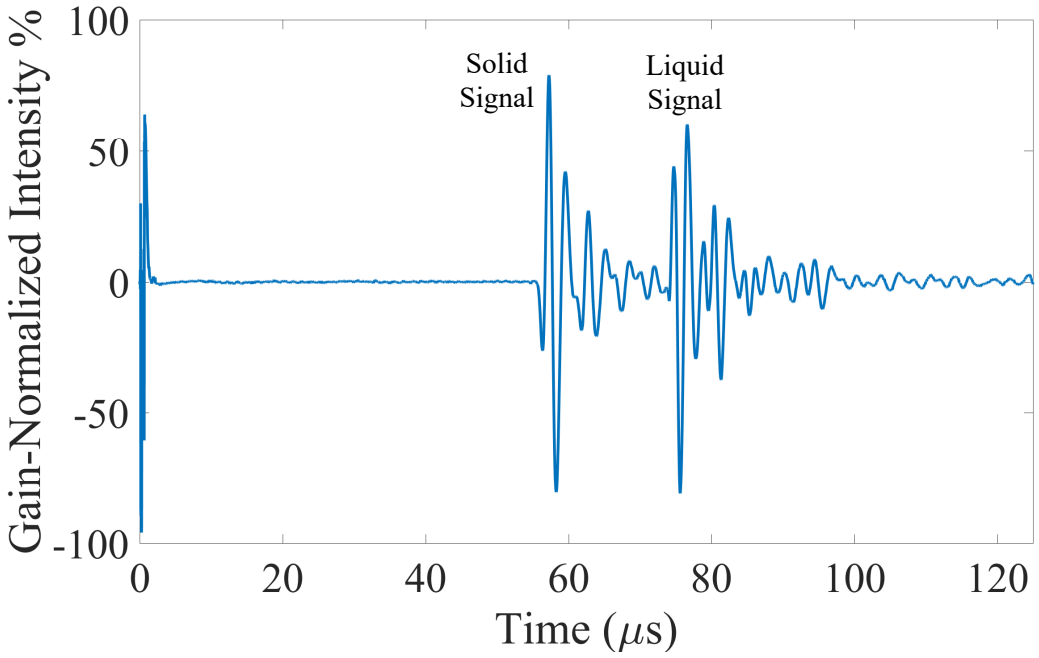

Figure 4.6. A-scan with both liquid and solid wax covering transducer face

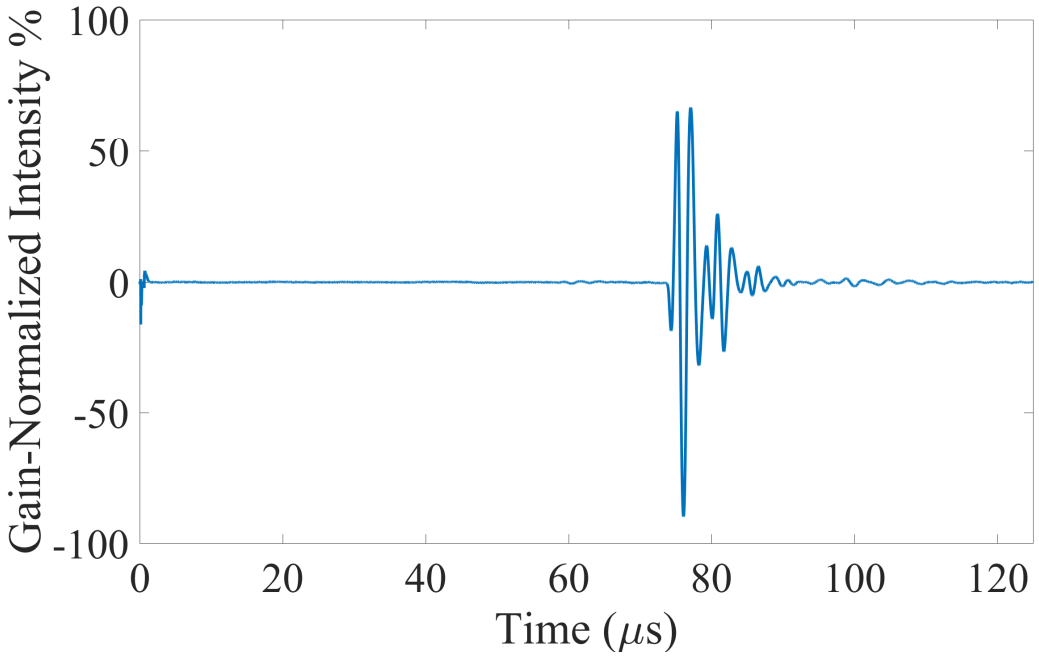

Figure 4.7. A-scan with liquid wax covering entire transducer face

By visually analyzing the shape of the collected A-scan, the phase of material covering the face of the transducer can be inferred. This technique is quite useful when the melt front propagates perpendicular to the scanning direction such that the transducer scans liquid and solid wax simultaneously. Because this method is relatively unreliable in regards to changing scanning perspective and depends on the visual analysis of a skilled technician or engineer, other phase change identification methods were sought that could be determined more easily.

4.3.1.2 Speed of Sound Monitoring

After calculating the bulk speed of sound for each A-scan recorded throughout the heating and cooling of EcoSoya wax using Equation 1, a speed of sound curve with respect to experimental time was constructed for each ultrasonic channel, as shown in Figure 4.8.

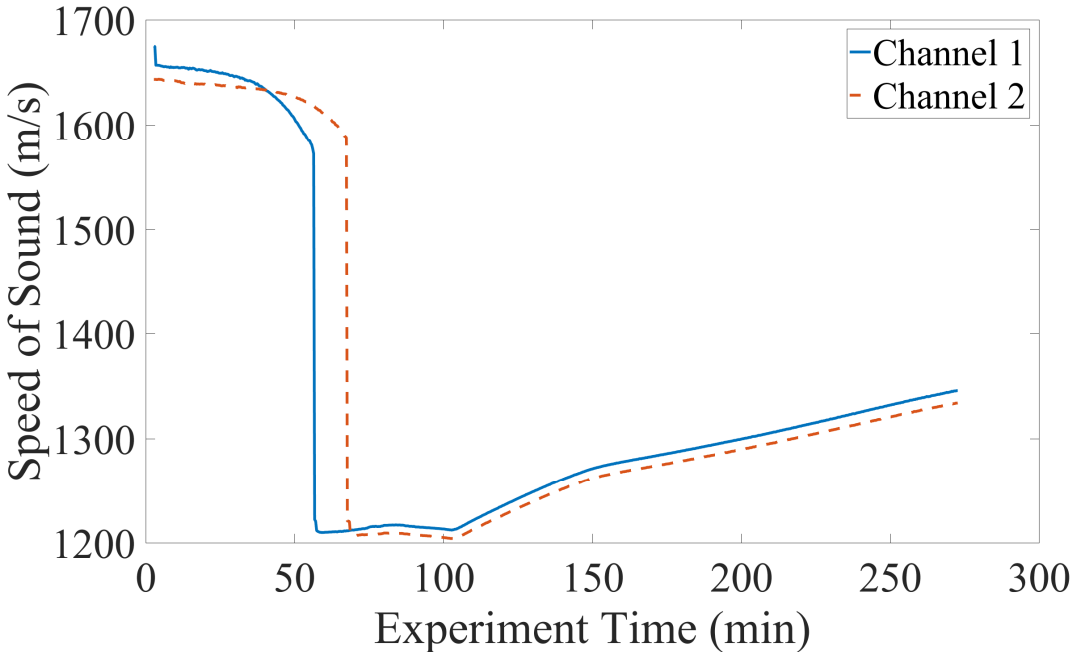

Figure 4.8. Speed of Sound Data for All Channels

Important phase data can be determined visually using speed of sound monitoring. Speed of sound data from Channel 1, closest to the heating block, is shown in Figure 4.9 with important regions and points labeled. Using this figure, the wax can be shown to be in a solid state between 0-55 min because of its high speed of sound and is marked as region (i) in Figure 4.9. Between regions (i) and (ii), there is a drastic drop in the speed of sound to approximately 1000 m/s, indicating a phase change from solid to liquid has occurred. Because the material is then at a steady temperature in region (ii) while in a liquid state, the speed of sound is relatively constant and remains at this level until the heater is turned off at 110 min. Following this, the wax begins to cool in region (iii) as the speed of sound slowly increases while the wax transitions back to a solid until the experiment is over.

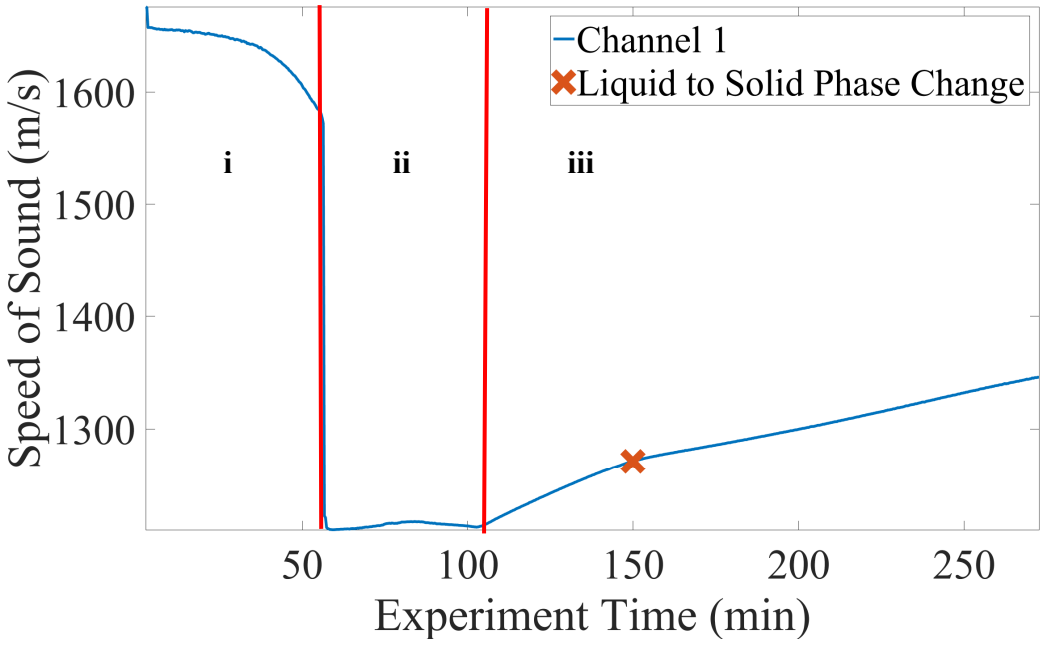

Figure 4.9. Speed of sound data for channel 1 with heating, constant temperature, and cooling regions labeled i, ii, and iii, respectively. Solid to liquid and liquid to solid phase changes occur at events A and B, respectively.

Additionally, a kink can be seen at 150 min, indicating a phase change from liquid to solid. The solid to liquid transitions occurred during heating at different times, 56 min and 67 min for Channels 1 and 2, respectively, as shown in Figure 4.8. Conversely, the liquid to solid transitions occur nearly simultaneously, approximately 150 min into the test. The difference in times of phase change from solid to liquid is due to the melt direction and the 5 cm separation between scanning channels, as shown in Figure 3.17. Because the box is cooled through convection on the top surface of the acrylic box, the temperature state on any horizontal plane is essentially a constant during cooling. Thus, the liquid to solid phase transitions occur at the same time throughout the box on any given horizontal plane. In this way, speed of sound monitoring can be used to identify the material state and detect phase changes in EcoSoya wax.

An ultrasonic B-scan with the independent variable being experimental time instead of the traditional spatial placement of the transducer is also quite useful in the identification of material state. An ultrasonic B-scan is an imaging technique to visualize many A-scans at once. All A-scans taken throughout the test are aligned next to each in Figure 4.10 other where the x-axis is experimental time, the y-axis is gate time of the ultrasonic scan, and the z-axis, shown in normalized intensity, is amplitude of the A-scan.

The time of flight can be estimated using Figure 4.10, as the onset of the signal is indicated by the horizontal black line, initially appearing between 0 and 50 min at approximately 60 μs. Thus in region (i) the gate time where the signal first occurs is 55 μs, whereas in region (ii) the gate time where the signal first appears is 75 μs. Region (iii) identifies the cooling period.

Similar to that of the speed of sound data shown in Figure 4.8, a kink is observed at 110 minutes, corresponding to the moment in time that the heater is turned off. A second change in the curve's inflection, though less obvious, occurs at 150 min, corresponding to the moment that the wax changes from liquid to solid. An additional advantage of B-scan imaging is the ability to see the liquid signal grow in intensity, as shown in region (iv). The physical reason for this signal lengthening in gate time between experimental time of 40 and 55 min is the liquid wax moving to cover the face of the transducer and the growing prominence of the liquid signal in relation to the solid signal, at approx. 55 μs. See Figure 4.13 for further details. Signal growth as shown in Figure 4.10 provides valuable information on estimating the rate of melt.

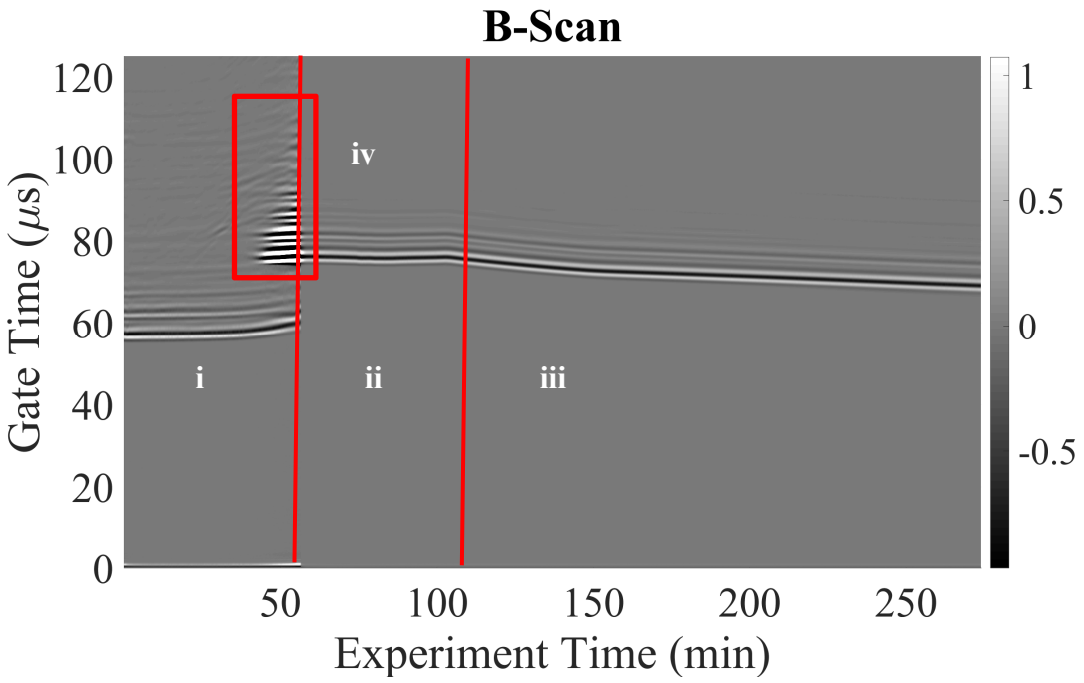

Figure 4.10. Ultrasonic B-scan with respect to time. The liquid signal can be seen growing in region iv. Regions i, ii, and iii from Figure 4.9 can also be seen.

4.3.1.3 Electrical Gain Tracking

In addition to material speed of sound monitoring, electrical gain tracking can be used to identify phase changes from solid to liquid. The gain values required to maintain the signal at a specific peak signal intensity threshold of 95% of gain-normalized intensity as discussed previously are shown below in Figure 4.11.

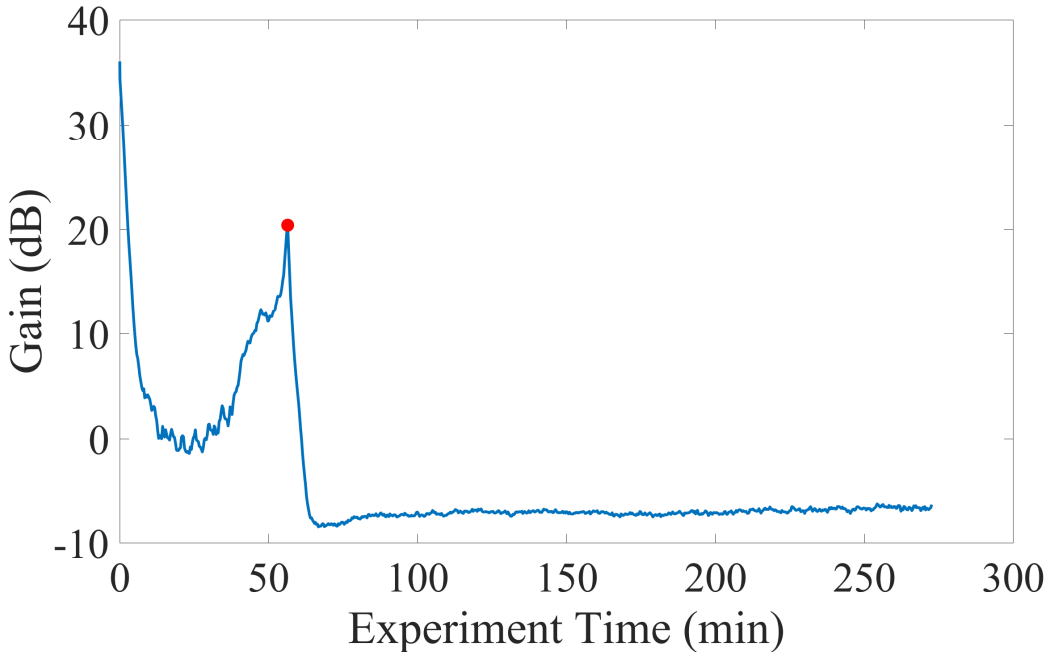

Figure 4.11. Gain as a function of experiment time with solid to liquid phase change marked with a red dot.

The local maximum occurring at 55 min into the test indicates a solid to liquid phase change occurring. The physical reason for this peak in gain value can be seen in Figure 4.12, Figure 4.13, and Figure 4.14. Figure 4.12, similar to Figure 4.6, shows an ultrasonic A-scan prior to the gain peak at 55 min, when the transducer face is covered by both solid and liquid wax. As the liquid wax begins to cover more of the transducer face, the signal amplitude of the liquid signal grows in amplitude. While a solid signal is present in the A-scan, the LabVIEW program corrects the gain so that the "solid signal" is held at the set threshold. Once the solid signal no longer exceeds the detection threshold set in the LabVIEW code, the gain is then corrected based on the liquid signal. Because the "liquid signal" has a significantly higher amplitude, as shown in Figure 4.13, the gain must decrease in order to achieve the 95% saturation threshold. The dependence

of gain on material phase gives rise to the gain peak occurring at 55 min into the test. It is important to note that the gain peak, like the phase change identified by speed of sound monitoring, occurs at the moment the liquid wax completely covers the transducer face. This observation has been confirmed with a visual analysis of the test apparatus itself as the wax front is clearly visible in the acrylic box.

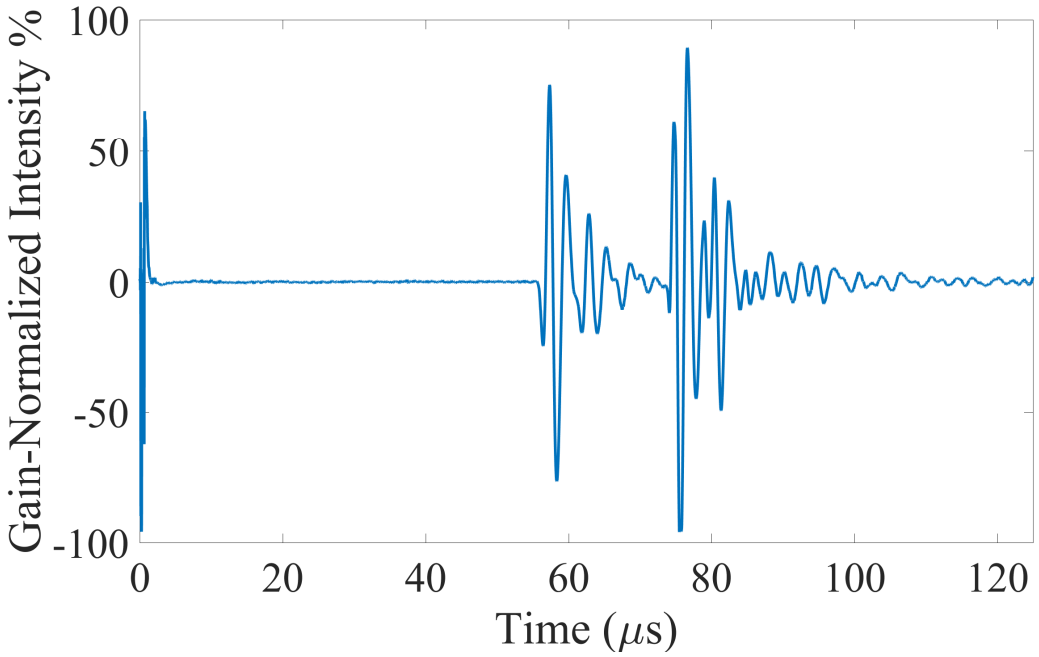

Figure 4.12. A-scan before gain peak

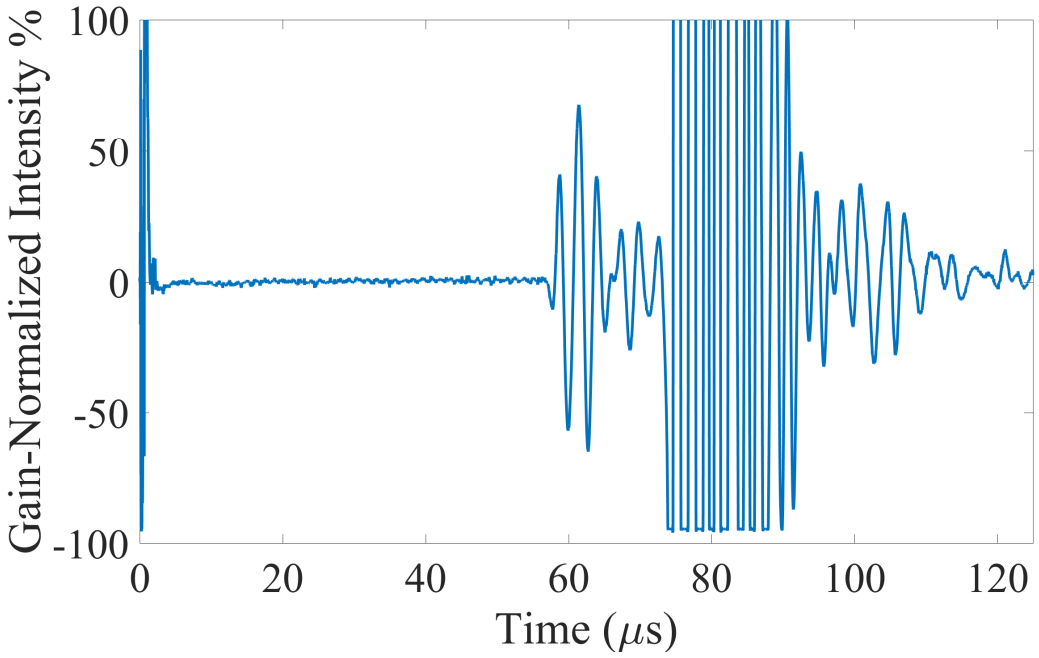

Figure 4.13. A-scan during gain peak

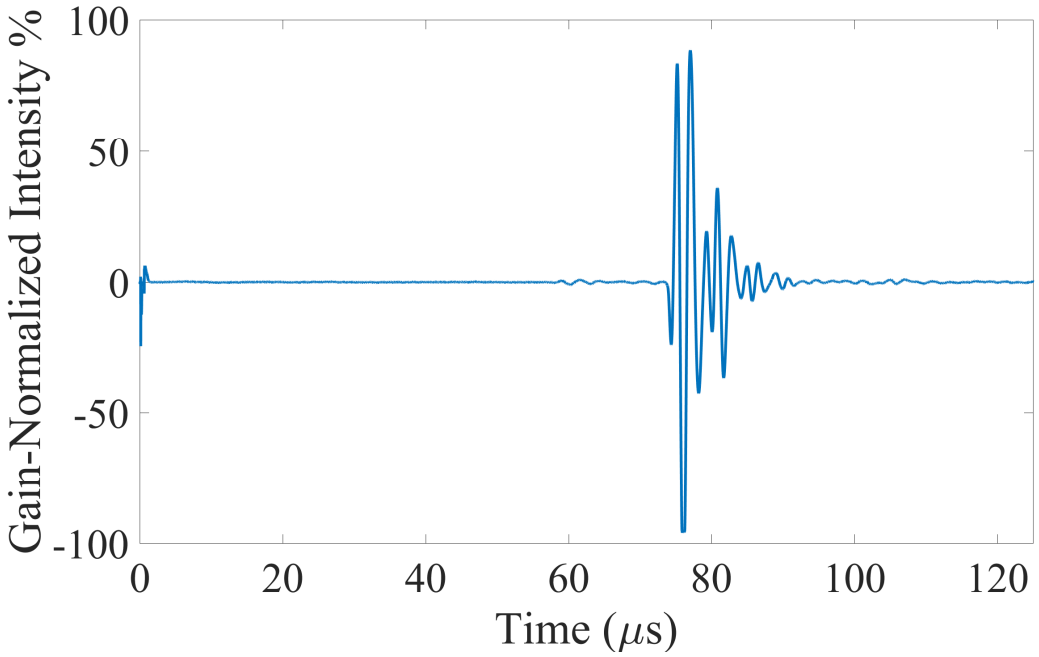

Figure 4.14. A-scan after gain peak

4.3.1.4 Frequency Analysis

Frequency analysis has also been investigated for determining phase changes in EcoSoya wax. Frequency analysis is performed in MATLAB by analyzing the solid and liquid signals contained within an A-scan. Signals are gated automatically in a MATLAB script based on time of flight of the A-scan. An example of the frequency gating is shown in Figure 4.15.

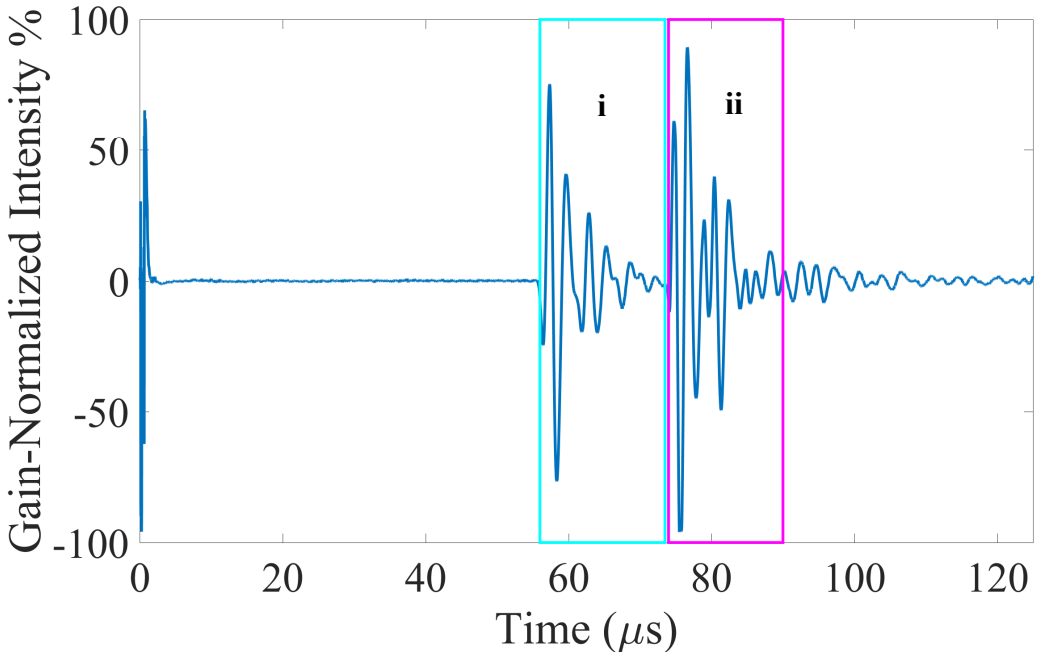

Figure 4.15. Frequency Gating of A-scan. Solid and liquid gates in red (i) and green (ii), respectively.

Using the A-scan data contained within the gates indicated in Figure 4.15, a frequency spectrum can be created from the coefficients in the Fourier Series. A Fourier Series decomposition is rooted in the idea that a waveform can be represented as a series summation of sines and cosines of various amplitudes. The amplitude coefficients and

frequencies of these sines and cosines are represented in the frequency spectrum of a signal. The frequency spectrum for the A-scan shown in Figure 4.15 is shown in Figure 4.16 for both the solid and liquid portions of the A-scan.

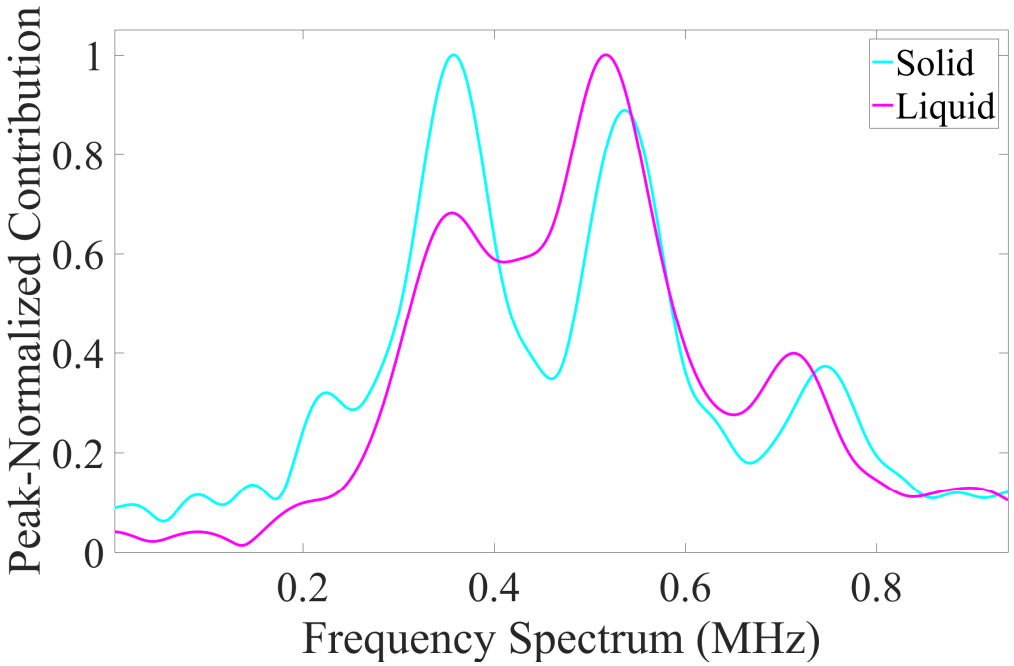

Figure 4.16. Liquid and Solid Signal Frequency Spectrum

An important difference between the solid and liquid frequency spectra can be observed in Figure 4.16 and can be used to identify phase changes in EcoSoya wax. The solid signal frequency spectrum, shown in blue, has two approximately even peaks at 0.3 MHz and 0.5 MHz, whereas the liquid signal spectrum has a much less significant local maximum at 0.3 MHz and a dominant peak at 0.5 MHz. The liquid wax can be thought of as a mechanical high-pass filter of the ultrasound wave, only letting through the high frequency components and absorbing the lower frequency components. Because of this, the author hypothesizes that the high frequencies attenuate faster in the solid material. In

this way, frequency spectra can be used to differentiate between liquid and solid wax signals.

The frequency spectrum as a function of experiment time, shown in Figure 4.17 and Figure 4.18, are used to visualize all frequency spectra over the course of a heating and cooling experiment. These plots show experimental time on the x-axis, frequency on the y-axis, and peak-normalized intensity of that frequency on the z-axis represented by the color.

In Figure 4.17, the solid to liquid phase change can be observed at 55 min. This can be identified because of the two dominant peaks shown in yellow occurring at 0.3 MHz and 0.5 MHz terminate at 55 min, marked by a vertical red line. In Figure 4.17, region (i) reflects the pattern observed in Figure 4.16, whereas in region (ii) there is no meaningful data recorded. The lack of any discernible pattern in region (ii) is due to the lack of a recorded solid signal in that time region (see e.g. Figure 4.14) and the analysis of only high-frequency noise above the 1 MHz shown in Figure 4.17.

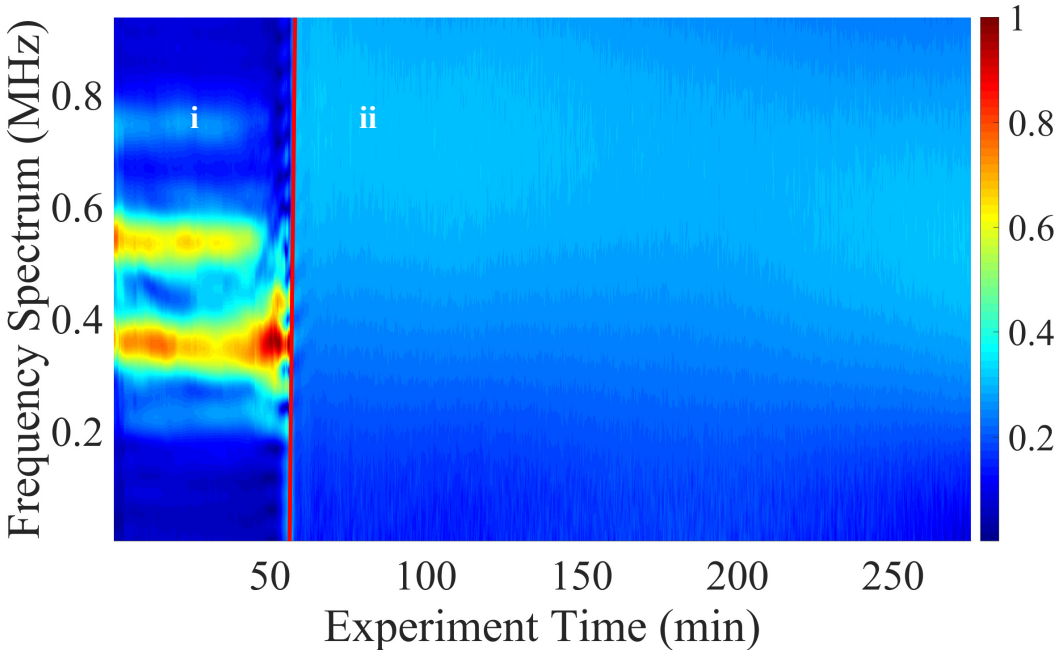

Figure 4.17. Solid Signal Frequency Spectra Surface Plot

Figure 4.18 can be used to identify the phase state of the wax based on the gate placed around the anticipated liquid signal. At 55 min the signal has only one distinct peak at approximately 0.5 MHz. This, as demonstrated in Figure 4.16, indicates that the wax is in a liquid state. The liquid to solid phase change, occurring between 150 min and 200 min, can be identified using Figure 4.18. This phase change can be identified because the two peaks reach approximately the same intensity value between 150 min and 200 min.

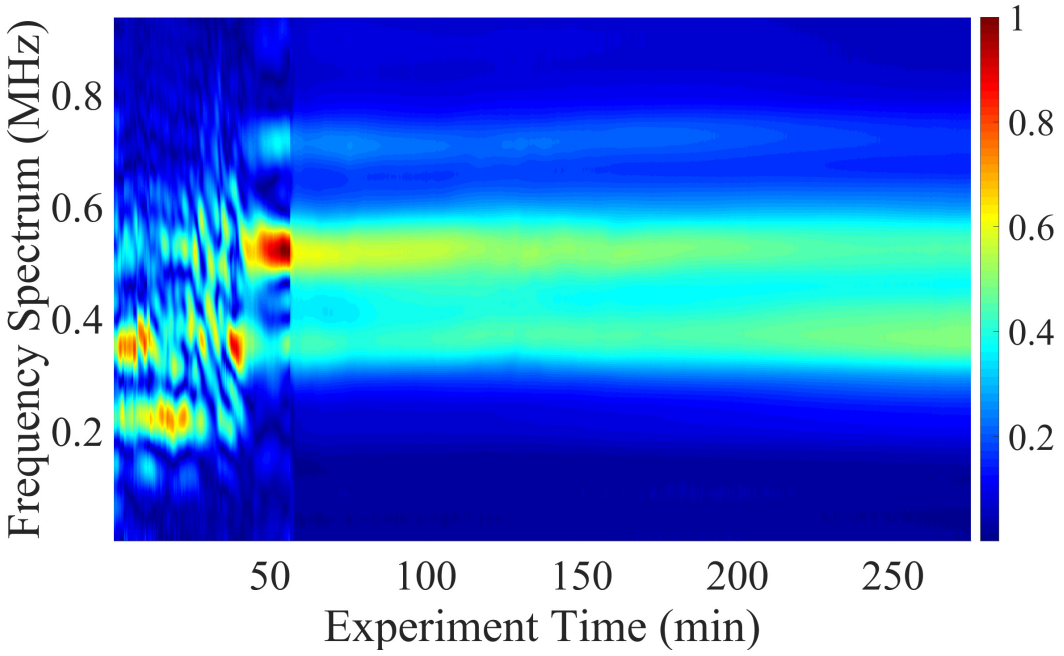

Figure 4.18. Liquid Signal Frequency Spectrum Surface Plot

Visualizing the frequency spectra calculated from A-scans is useful, but may be difficult to use to monitor phase changes algorithmically. A method of frequency spectrum analysis was sought which could be employed using a computer to detect phase changes. The kurtosis, the fourth moment of a distribution, is studied to quantify changing frequency spectra similar to that from [39] for damage detection in composites. In simple terms, kurtosis indicates the sharpness of a peak of a distribution. Thus, the higher the value of kurtosis, the sharper the frequency spectrum peak.

Before kurtosis could be calculated, a frequency spectrum, such as that shown in Figure 4.16, is discretized by approximating it as a distribution rather than a function. This was done by assigning a number of vertical bins proportional to the contribution value at a particular frequency. After this was performed, kurtosis, κ, could be calculated using

$$\kappa = \frac{\sum_{i=1}^{n}(f_i - \bar{f})^4}{n\sigma^4} \tag{4}$$

where $\bar{f}$ is the mean frequency value, f_i is the ith frequency value, σ is the population standard deviation, and $\Sigma_{i=1}^{n}$ is a summation from 1 to n, and n is the number of unique frequency bins of the quantity in the numerator. Figure 4.19 shows the calculated kurtosis value for each frequency spectrum in Figure 4.17, calculated as a function of experimental time.

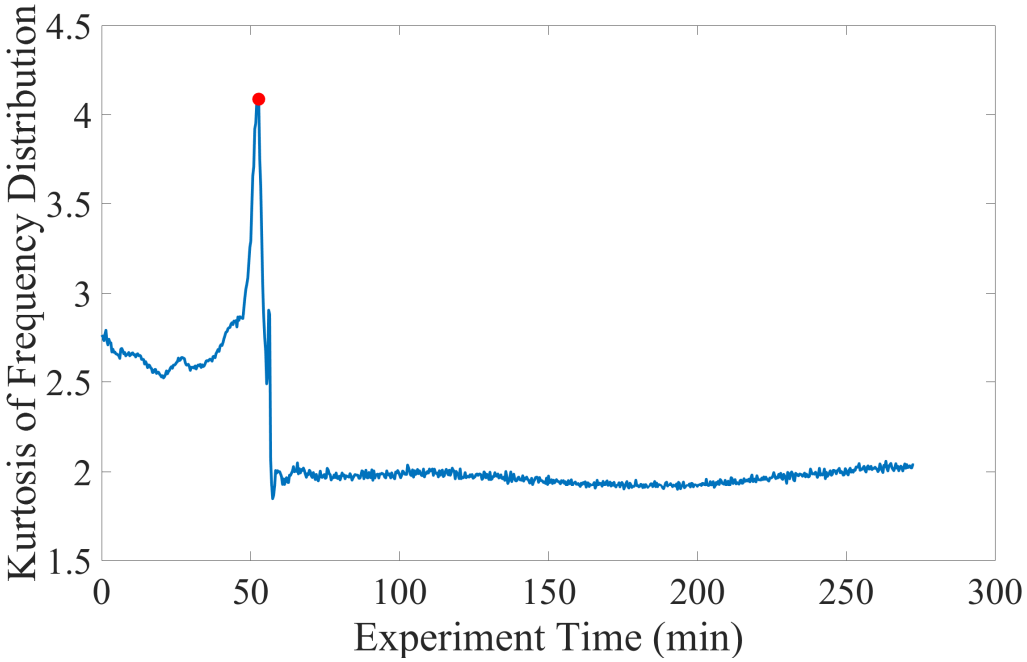

Figure 4.19. Kurtosis plotted as a function of experimental time

As can be seen in Figure 4.19, the value of kurtosis shows a clear peak at 55 min, when both the solid and liquid signals occur in the a-scan waveform. This is the same time the solid to liquid phase change was identified using other methods of phase change identification. Using this method, phase change can also be identified through a single parameter. This is particularly useful for automatic identification and has many potential applications in process controls and quality control scenarios.

4.3.2 EcoSoya Phase Change Method Summary

EcoSoya wax was used to identify and develop phase change detection methods. Using speed of sound, gain tracking, and frequency spectrum analysis, phase changes were successfully identified. Table 4.1 presents the summary results of each detection method. Using this table, it can be seen that all presented methods were able to identify the solid to liquid phase changes within a close band of time, confirming the validity and precision of each independent detection method. Discrepancies in time are due to the experimental configuration where the signal itself will pass through both a liquid and solid region of wax for several minutes. However, the estimated liquid to solid phase change occurs with a much wider time band bounding the phase change. It is important to consider that each method functions as a different method to capture solidification.

Table 4.1. Phase Change Method Comparison

ID Method	Calculated Melt Time (min)	Calculated Solidification Time (min)
A-scan Shape	57	N/A
Speed of Sound	57	~150
Gain Tracking	57	N/A
Frequency Analysis	52	150-200

4.4 Temperature Measurement

Using through transmission ultrasound, the temperature of EcoSoya wax was able to be measured by monitoring speed of sound of the wax. Thermocouples, inserted into the wax to reliably measure the temperature of the wax at specific points, provide temperature data that can be compared to the EcoSoya wax. Figure 4.20 shows the speed of sound data collected and shown in Figure 4.8 now plotted with respect to temperature measured by the thermocouples as the wax cools for the rectangular box configuration of Figure 3.19. It is important to note that the temperature of the wax between the transducers was calculated by first averaging the temperatures recorded by each row of thermocouples on one side of the ultrasonic path, doing the same with the row on the opposite side, and averaging the two results to interpolate and find the temperature at which the phase change is occurring.

Figure 4.20 shows only the cooling portion of the experiment. Examining this region, it can be seen that there is a 1-to-1 mapping between EcoSoya internal temperature as measured the thermocouples and the speed of sound measured using ultrasound. This monotonic relationship between speed of sound and temperature has important implications for the capabilities of this method, namely the ability to

reconstruct temperature profiles using tomographic techniques such as those discussed in Chapter 2.

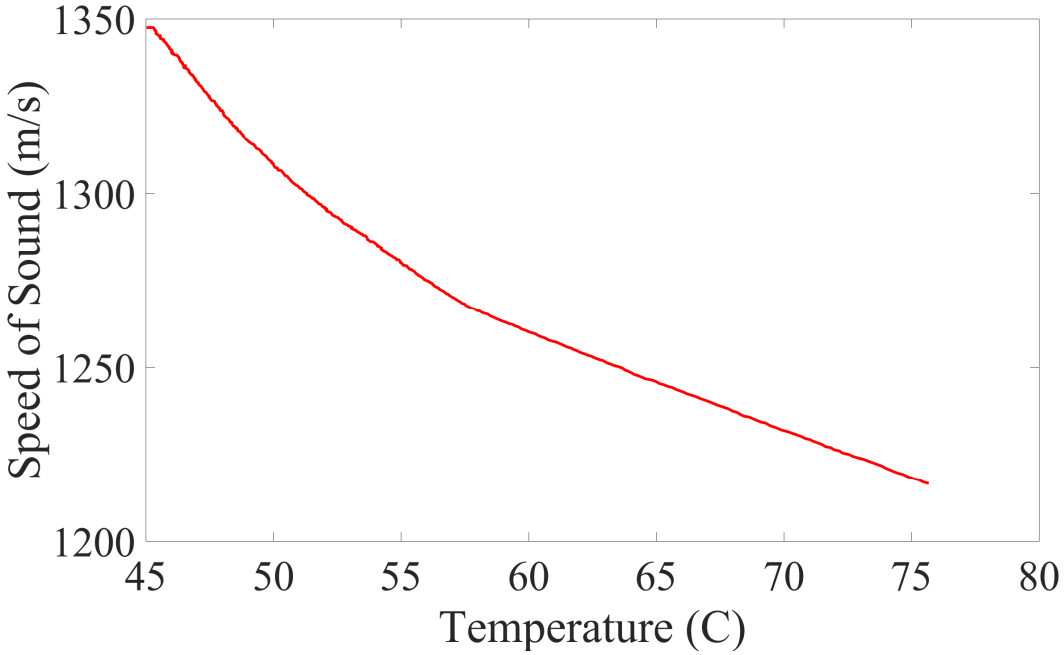

Figure 4.20. Speed of Sound vs. Temperature as EcoSoya wax cools.

As can be seen in Figure 4.20, a kink occurs at approximately 54 °C as the wax cools, indicating the solidification of the wax. This is in agreement with DSC test results shown in Figure 4.1, demonstrating the capabilities of this method.

Because of the potential to reconstruct temperature profiles in EcoSoya wax using ultrasonic techniques, an experiment was performed to determine the speed of sound profile of EcoSoya wax. This was done by equilibrating the wax at a set temperature well-above the melting point of the wax using a furnace. After this was done, the wax was allowed to cool and a speed of sound profile for EcoSoya wax was constructed by scanning the wax as it cooled. Results from this study are shown in Figure 4.21.

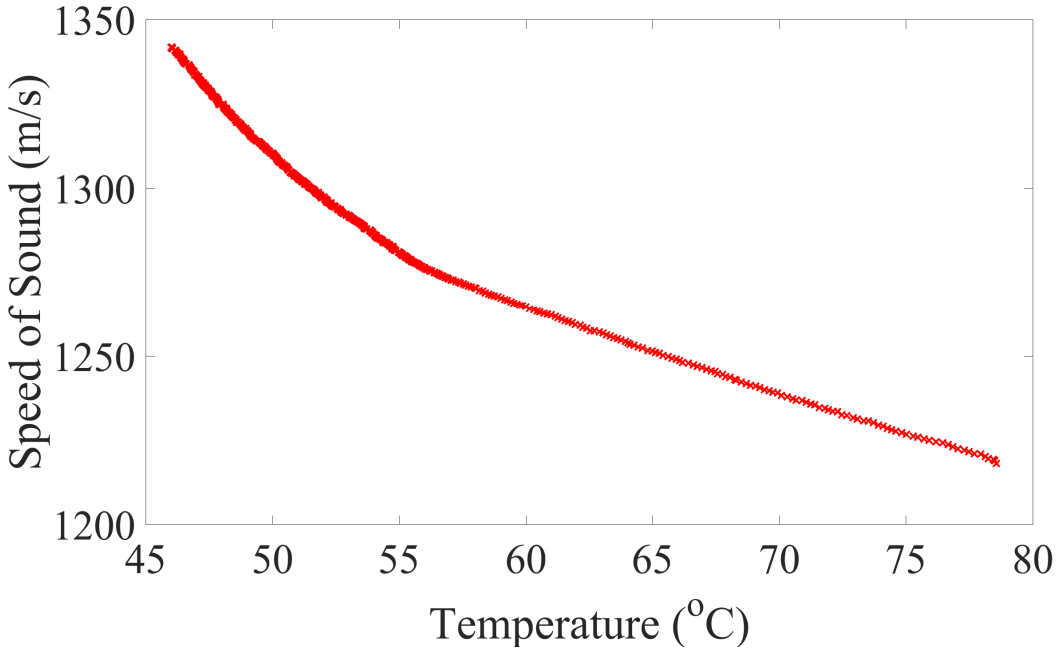

Figure 4.21. Speed of Sound study-EcoSoya wax

After results were obtained from this study as shown above, it was determined that a piecewise-linear curve fit would be the best model to represent the speed of sound of EcoSoya wax. Results from the curve fit are shown in Figure 4.22.

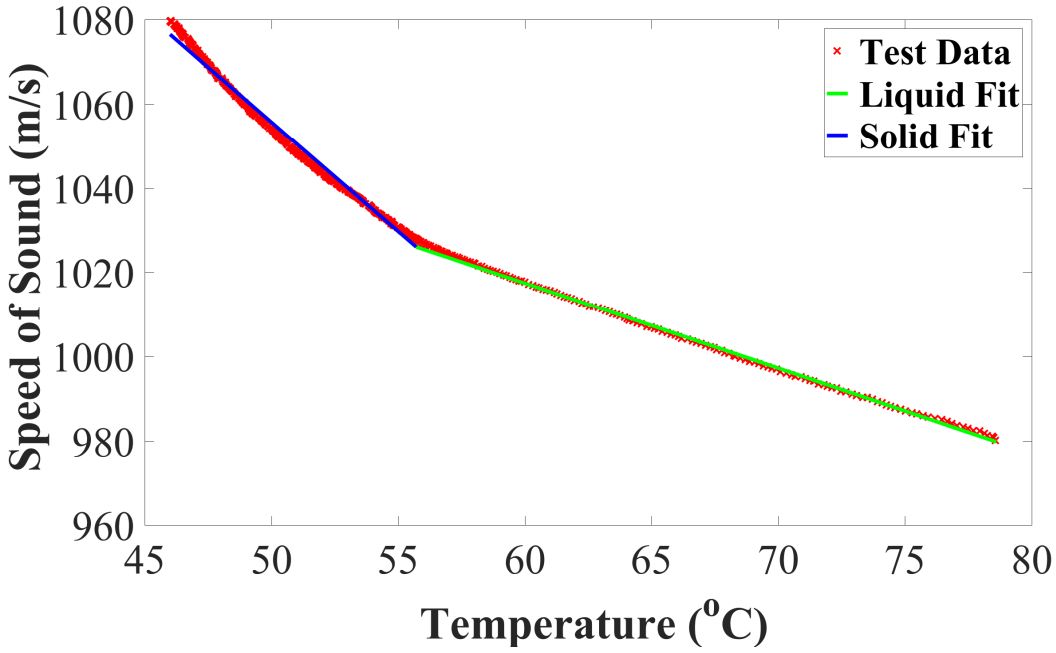

Figure 4.22. Curve fit to EcoSoya Speed of Sound Profile.

4.4.1 EcoSoya Phase State Imaging

As a result of knowledge of the speed of sound profile of EcoSoya wax, a phase state image reconstruction method was created. To do this, the cylindrical geometry experimental apparatus shown in Figure 3.20 was used. A further assumption regarding speed of sound in different phases was employed as a first attempt at imaging material phase. The piece-wise linear speed of sound vs. temperature profile was approximated as a step function where the temperature of solid wax has a high speed of sound and the liquid wax has a low speed of sound. The step occurs where the phase transition was determined to occur on the basis of the curve fit, 55 °C. This speed of sound approximation is shown in Figure 4.23.

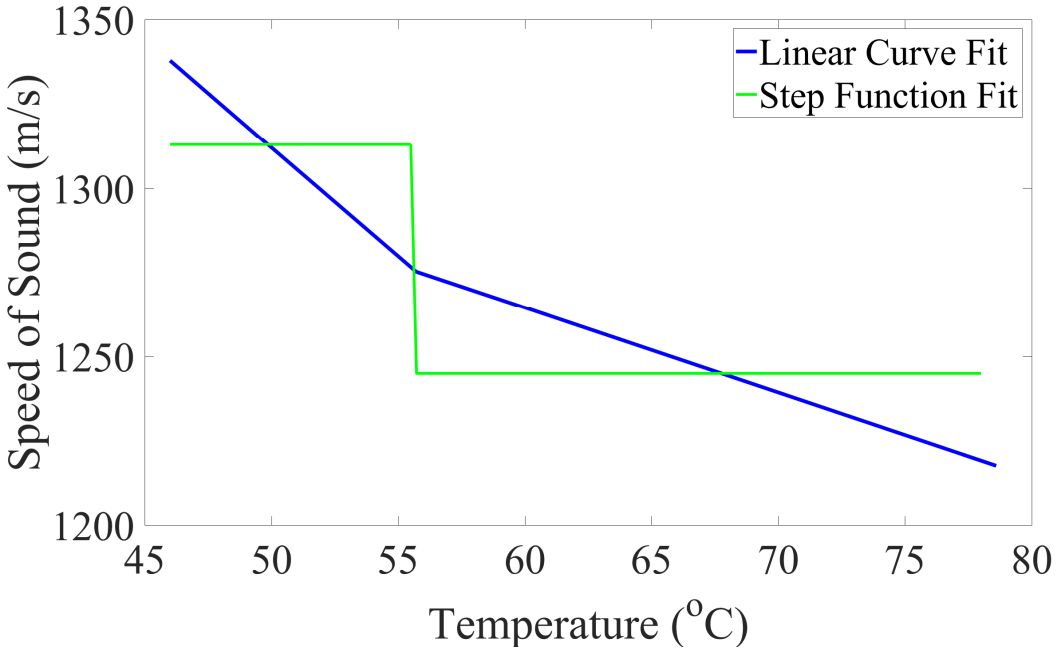

Figure 4.23. Step function speed of sound approximation.

As a result of approximating the speed of sound vs. temperature profile as a step function, it is possible to create a binary phase state estimation image using a circular array of ultrasonic transducers. A further requisite for this imaging technique is the knowledge that wax begins in a known solid state.

The binary phase imaging technique hinges on the basis that sound travels at different speeds in liquid and solid wax. A binary image is created by measuring the speed of sound while the material melts and, because solid and liquid speeds of sound are known, calculating the fraction of travel time the sound spends in liquid wax. Because the wax is center-heated, it can be assumed that the liquid wax is in the center of the cylinder of wax. Calculations to determine the amount of time the sound spends in liquid wax are performed using Equation 5,

$$t_L = \frac{\left(t_{Total} - \frac{2r}{v_{Solid}}\right) v_{Solid} v_{Liquid}}{v_{Solid} - v_{Liquid}} \tag{5}$$

where t_{Total} is the time of flight, r is the radius of the bucket, and v_{Solid} and v_{Liquid} are the step-wise approximated velocities in solid and liquid wax, respectively. By calculating the distances traveled in solid and liquid wax across multiple channels a phase plot can be created. It should be noted that this technique, with enough transducer channels, can resolve non-axially symmetric melt patterns. This was demonstrated using theoretical data. Results of this theoretical test are shown in Figure 4.24.

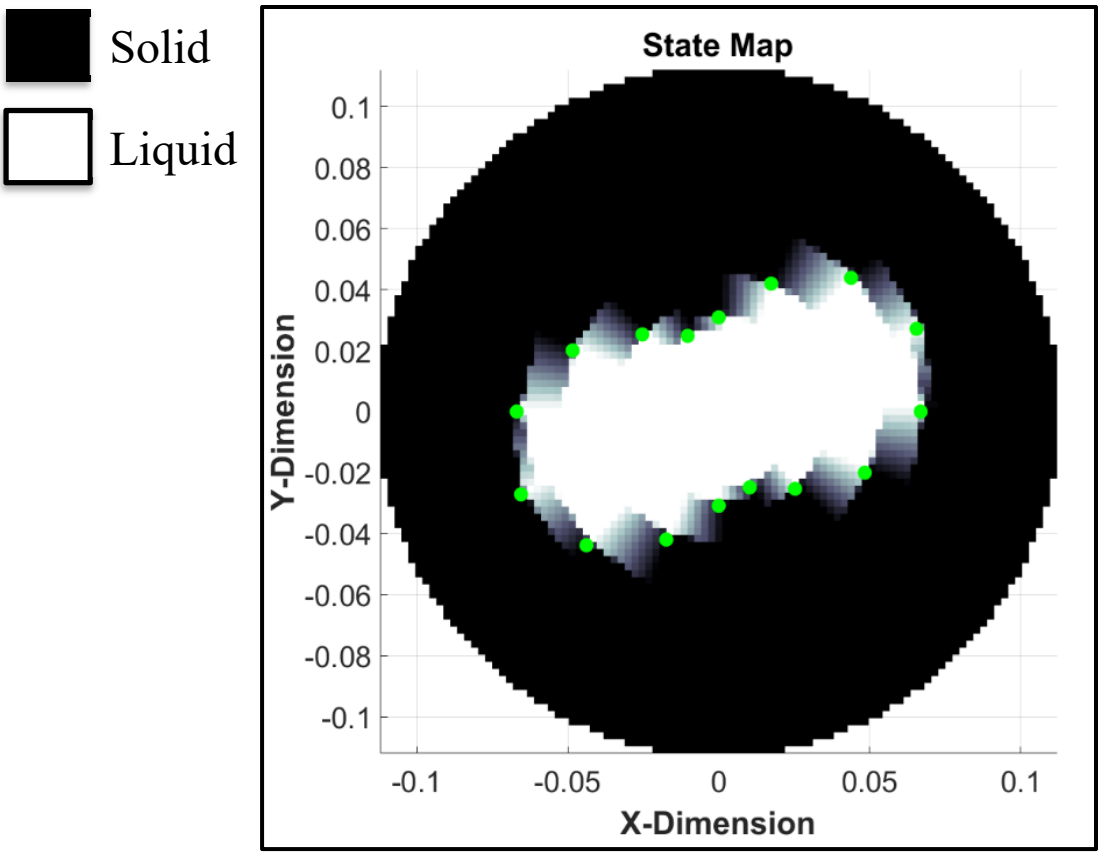

Figure 4.24 . Non-axially symmetric binary phase plot.

Once the binary phase imaging technique was tested using theoretical data on the computer, an experimental validation was performed. This was done using the cylindrical geometry apparatus with a heater in the center 3 in. from the bottom. Results from the experimental validation are shown in Figure 4.25, Figure 4.26, and Figure 4.27.

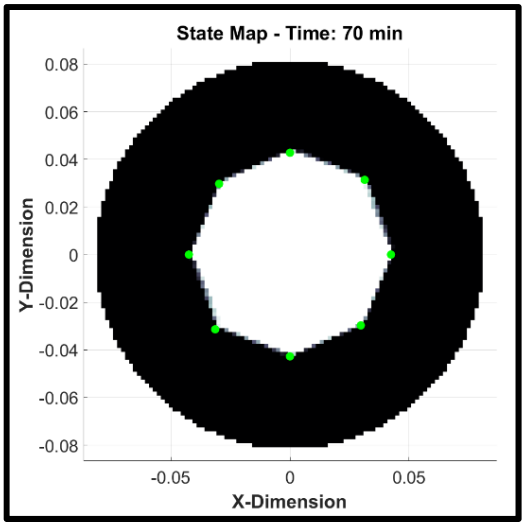

(a)

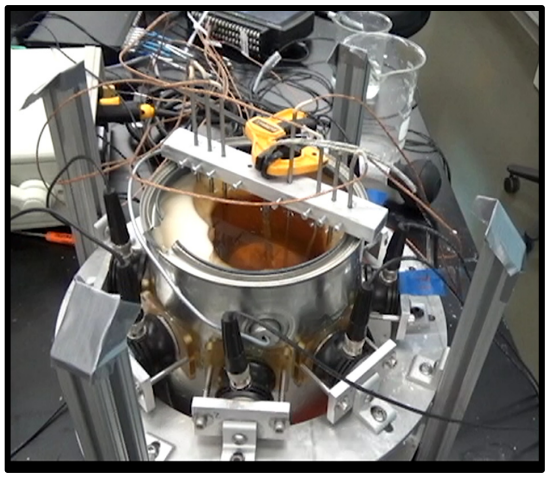

(b)

Figure 4.25. Binary Phase State Imaging Experimental Study: 70 min

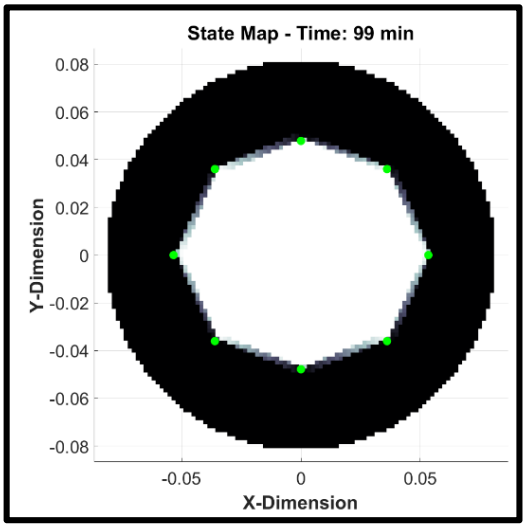

(a)

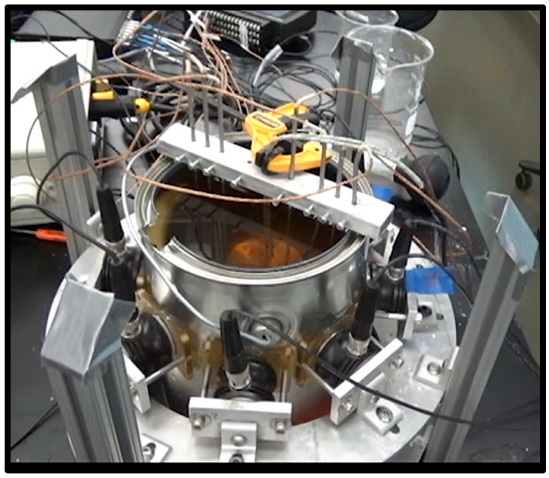

(b)

Figure 4.26. Binary Phase State Imaging Experimental Study: 99 min

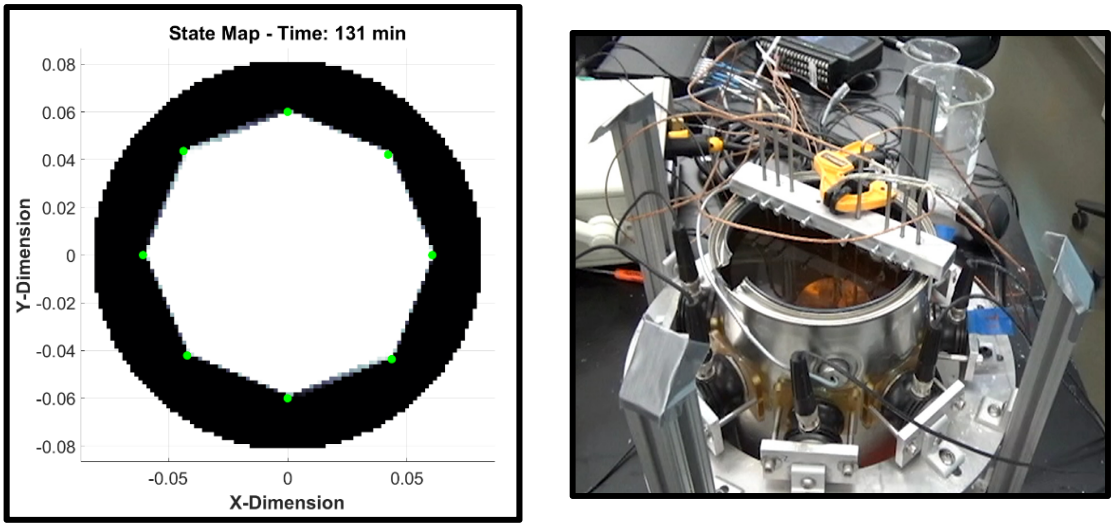

(a) (b)

Figure 4.27. Binary Phase State Imaging Experimental Study: 131 min

As can be seen in the above figures, the binary phase state imaging technique performed well in the experimental study, with images created only from ultrasound information accurately reflecting the binary phase state of the EcoSoya wax. Figure 4.25(b) shows the wax as it melts, where the solid wax can be seen in the lighter color on the left side of the bucket and the darker, liquid wax on the right center. Figure 4.26(b) shows the bucket 29 min later with a small part of solid wax just visible in the plane of the left-most transducer. This small part of solid wax is still detected by the phase imaging technique and is evident in Figure 4.26(a). Discrepancies in exact location and size of the liquid and solid wax boundary can be seen in Figure 4.25(a) where the liquid wax boundary is assumed to be symmetrical about the centerline of the bucket, in the phase imaging, but the wax boundary depicted in part (b) of the same figure shows the wax boundary slightly off-center.

Although the created images are not an exact representation of the physical state of the wax, the phase imaging technique provides valuable insight into the heating pattern of the wax. This could be particularly valuable in situations where the inside of the container is completely blocked off from viewing. Additionally, situations where the outside perimeter of the material is solid and thus the container is cool to the touch but the inside is relatively hot would be a particular strong suit of this imaging technique.

CHAPTER FIVE:

CONCLUSIONS AND FUTURE WORK

5.1 Conclusions

As polymers and other complex material systems become more prevalent in applications in such industries as automotive, aerospace, and energy generation, the need for methods to understand and characterize the internal temperature state of these materials is increasing. Ultrasound is one set of nondestructive inspection techniques that may be used for these purposes.

In this thesis, through experiments of heating and cooling of a semi-crystalline material, specifically EcoSoya wax, techniques were developed to detect phase changes and the internal temperature state for this material. Several novel phase change identification methods were introduced, including speed of sound monitoring, electrical gain tracking, and frequency analysis. Using speed of sound monitoring and knowledge of the speed of sound characteristics of the material of interest, a binary phase detecting imaging process was developed in this thesis.

In the area of internal temperature monitoring, time of flight monitoring was employed to characterize the speed of sound versus temperature characteristics of EcoSoya wax using an experimental procedure designed to characterize the acoustic properties of materials, detailed in Section 4.2.1, which could be extended to characterize other, similar materials. Due to the similar thermal behavior of EcoSoya wax many thermoplastic polymers, as demonstrated during DSC testing (see Section 4.1.1), the author hypothesizes that similar techniques to those outlined in this work can be

employed on similar material systems. Similar material systems would likely be those that experience phase changes over a range of temperatures and lack a defined material structure. The author proposes that work in expanding these techniques and developing new ones will contribute to the further understanding of these materials.

5.2 Scientific Contributions

The novel contributions of this thesis lie in the study of amorphous and semi-crystalline materials undergoing phase changes. Work has been performed in the area of temperature monitoring on polymers in the past, as described in Chapter 2, however, little work has been done studying the acoustic properties of these amorphous and semi-crystalline materials as they change phases. Multiple methods such as A-scan shape, speed of sound monitoring, electrical gain monitoring, and frequency analysis, all discussed in Section 4.3.1, were developed for identifying the melt transition of a semi-crystalline material. These methods confirmed the measurements of each other and are rooted in independent phase change identification methods and, when used in combination, provide confidence in the identification of phase changes. Validation of these techniques was performed by comparing results to DSC testing, and is presented in Figure 4.1. Similarly, both 1-D and 2-D presentations of the internal phase of a material were developed using ultrasound. The 1-D presentations, the charts created for the four phase change identification techniques listed, provide insight into how the phase state of the material of interest varies between two transducers. The 2-D presentation, the binary phase state imaging technique employed in this work and compared qualitatively with experimental observations (see e.g. Figure 4.25) has the potential to provide a technique to understand and predict the melt pattern of amorphous and semi-crystalline materials.

The two-dimensional presentation may provide for a more detailed and intuitive understanding of results. These methods for identifying melt transitions and imaging phase state provide for an understanding of the phase state characteristics of EcoSoya wax using only ultrasound. Knowledge of the material state of EcoSoya wax gained through these phase state imaging techniques can be used for informed improvement of processing techniques for similar categories of materials, such as injection molding and polymer extrusion of thermoplastics.

The automatic gain-adjustment algorithm implemented using in-house LabVIEW code provides a method for improved ultrasonic scanning. Not only does the developed LabVIEW program provide a procedure for characterizing materials undergoing phase changes using ultrasonic testing, but provides for capturing the maximum data resolution of the generated ultrasonic signals. The improved data resolution of signals using the gain-adjustment algorithm supports the research done in this study and enhances previously-developed ultrasonic techniques for phase detection and temperature imaging. Certain techniques such as frequency analysis are particularly dependent on the available data resolution of a signal and can be significantly enhanced through the use of data with an optimal resolution. Using high-resolution data allows for enhanced understanding of material systems and improved analysis of collected signals.

Moreover, visualizations of temperature and melt state of a material were created and the relationship between speed of sound and material temperature was developed for EcoSoya wax. This speed of sound versus temperature relationship is key to the understanding of how the material behaves from the perspective of ultrasonics and can be used in support of further work outlined in the next section. An ultrasonic B-scan with

respect to time, shown in Figure 4.10, presents information both about the approximate temperature and the melt state of the material. This B-scan visualization provides valuable information for informed decision making for manufacturing and quality control processes.

5.3 Future Work

5.3.1 Phase Detection and Imaging

The goal of the phase detection and imaging work of this thesis was to develop techniques to monitor phase changes in amorphous and semi-crystalline materials. The above work demonstrates the feasibility of a diverse array of techniques such as speed of sound monitoring, gain monitoring, and frequency analysis as methods to detect phase changes in EcoSoya wax. The author proposes that further work be performed in this area to develop techniques that will provide innate understanding of amorphous and semi-crystalline materials undergoing phase changes. A-scan shape and gain monitoring, two phase change techniques outlined in this work, are constrained by the experimental setup to those in which the direction of the melt front propagates normal to the scanning direction of the ultrasonic transducers.

Additionally, the frequency analysis performed in this work can be further used to better understand the behavior of materials of interest in different phases. More complex frequency analysis methods beyond kurtosis and local frequency maxima, the two primary methods employed in this thesis, could be used for developing these techniques. One such method the author proposes is an analysis of attenuation. This could provide results useful for determining material phase. This study could be performed by taking the Fourier transform of a gated signal, inverting the resulting frequency signal with only

select frequency ranges back to the time domain, and analyzing how each signal attenuates. Using this method, attenuation as a function of frequency could be determined. By performing this sort of analysis for different material phase states, a relationship between frequency-based attenuation characteristics and material phase state. Understanding how the ultrasonic wave attenuates as a function of the wave frequency could be coupled with the overall frequency analysis for more accurate phase state determination.

With regard to the binary phase state imaging technique used in this work, using a more accurate approximation of the speed of sound versus temperature relationship would significantly improve the accuracy of the phase state imaging (see Figure 4.23). Additionally, the implementation of an accurate curve fit and associated imaging algorithm could be used to image more than simply solid and liquid wax and thus provide a better understanding of the melt front of the wax. The author hypothesizes that this improvement could lead to accurate imaging at lower temperature melting and the creation of a two-dimensional phase mapping of the material showing more than simply liquid and solid.

The author further proposes that a neural network approach be employed to determine the phase of a material by combining the above-mentioned techniques, similar to that presented in [8]. A neural network approach could allow for a trained algorithm to use several features of an ultrasonic wave such as attenuation characteristics, speed of sound, and kurtosis to determine phase state. A neural network, if properly trained, may be able to accurately determine phase at any point in the scanning process. Limitations of

this approach would be difficulties in training the algorithm and the material- or application-specific nature of neural networks.

5.3.2 Temperature Reconstruction

This thesis had the goal of understanding ultrasonic wave propagation in amorphous and semi-crystalline materials in different temperature states. The method employed in this thesis was to experimentally correlate speed of sound to material temperature. The ability to accurately monitor the temperature of EcoSoya wax in real-time using speed of sound has significant implications for the capability of this technique. Once the relationship between speed of sound and internal temperature of a material is known, two-dimensional temperature reconstruction techniques such as a least squares regression curve fit can be relatively easily implemented in order to gain a better understanding of the material state.

The author proposes that future work in the area of understanding wave propagation in the EcoSoya wax include a finite element study. Using finite element techniques, a multi-physics simulation encompassing acoustics as well as heat transfer elements can be used for the verification of experimental results and refinement of analysis techniques.

In addition to a finite element study, the author proposes that 2-D and 3-D temperature reconstruction algorithms such as those discussed in Section 2.2.2.2 be implemented in conjunction with phase imaging data. As an initial reconstruction, the author proposes the implementation of a least squares regression-based technique, which is created by minimizing the point-by-point curve fitting error (see e.g. [22]). To aid in achieving high reconstruction quality, the author proposes that more transducer paths be

implemented on the material testing system. The creation of 2-D and 3-D temperature distribution reconstructions would provide intimate understanding of heating and cooling processes in applications such as injection molding and polymer extrusions.

Limitations to the implementation of such techniques for applications such as injection molding or extrusion of polymers include the attenuation and scattering of the sound wave in the material, the ability to effectively couple ultrasonic transducers to the material, and accessibility of the material. However, a method for temperature measurement in solids using pulse-echo configuration and well-placed echogenic features was cleverly developed and outlined by Jia *et al.* [14]. The author hypothesizes that similar methods using implanted echogenic features could be implemented or developed to adapt the outlined phase detection and temperature measurement techniques to a pulse-echo configuration. Already, work is underway to develop and adapt current methods to pulse-echo setups.

BIBLIOGRAPHY

[1] Häupler, M., Peyronel, F., Neeson, I., Weiss, J., and Marangoni, A. G., 2014, "In Situ Ultrasonic Characterization of Cocoa Butter Using a Chirp," Food Bioprocess Technol., **7**(11), pp. 3186–3196.

[2] Gregg, C. M., "The Observation of Phase State and Temperature Using Noninvasive Ultrasonic Waves," Baylor University.

[3] Winkelmeyer, C. B., Peyronel, F., Weiss, J., and Marangoni, A. G., 2016, "Monitoring Tempered Dark Chocolate Using Ultrasonic Spectrometry," Food Bioprocess Technol., **9**(10), pp. 1692–1705.

[4] Halmen, N., Kugler, C., Hochrein, T., and Heidemeyer, P., 2017, "Ultrasound Tomography for Inline Monitoring of Plastic Melts," J. Sens. Sens. Syst., **6**(1), pp. 9–18.

[5] Brown, E. C., Olley, P., and Coates, P. D., 2000, "In Line Melt Temperature Measurement During Real Time Ultrasound Monitoring of Single Screw Extrusion," Plast. RUBBER Compos., **29**(1), pp. 3–13.

[6] Fei Yan, Royer, R. L., and Rose, J. L., 2010, "Ultrasonic Guided Wave Imaging Techniques in Structural Health Monitoring," J. Intell. Mater. Syst. Struct., **21**(3), pp. 377–384.

[7] Ren, B., and Lissenden, C. J., 2015, "Phased Array Transducers for Ultrasonic Guided Wave Mode Control and Identification for Aircraft Structural Health Monitoring," Mater. Eval., **73**(8), pp. 1089–1100.

[8] Barry, T., Kesharaju, M., Nagarajah, C., and Palanisamy, S., 2016, "Defect Characterisation in Laminar Composite Structures Using Ultrasonic Techniques and Artificial Neural Networks," J. Compos. Mater., **50**(7), pp. 861–871.

[9] Stair, S. L., 2014, "Non-Destructive Evaluation of Carbon Fiber-Reinforced Laminated Composites.," Thesis.

[10] Stair, S. L., 2017, "Nondestructive Inspection and Characterization of Complex Engineering Materials via Ultrasound Techniques," Baylor University.

[11] Chen, T.-F., Nguyen, K. T., Wen, S.-S. L., and Jen, C.-K., 1999, "Temperature Measurement of Polymer Extrusion by Ultrasonic Techniques," Meas. Sci. Technol., **10**(3), p. 139.

[12] Fujii, M., and Zhang, X., 2001, "Noncontact Measurement of Internal Temperature Distribution in a Solid Material Using Ultrasonic Computed Tomography," Exp. Therm. Fluid Sci., **24**(3), pp. 107–116.

[13] Jia, R., Xiong, Q., Xu, G., Wang, K., and Liang, S., 2017, "A Method for Two-Dimensional Temperature Field Distribution Reconstruction," Appl. Therm. Eng., **111**, pp. 961–967.

[14] Jia, Y., Puga, M., Butterfield, A. E., Christensen, D. A., Whitty, K. J., and Skliar, M., 2013, "Ultrasound Measurements of Temperature Profile Across Gasifier Refractories: Method and Initial Validation," Energy Fuels, **27**(8), pp. 4270–4277.

[15] Jia, Y., and Skliar, M., 2016, "Noninvasive Ultrasound Measurements of Temperature Distribution and Heat Fluxes in Solids," Energy Fuels, **30**(5), pp. 4363–4371.

[16] Liu, D., and Ebbini, E. S., 2010, "Real-Time 2-D Temperature Imaging Using Ultrasound," IEEE Trans. Biomed. Eng., **57**(1), pp. 12–16.

[17] Takahashi, M., and Ihara, I., 2008, "Ultrasonic Monitoring of Internal Temperature Distribution in a Heated Material," Jpn. J. Appl. Phys., **47**(5), pp. 3894–3898.

[18] Yuqian Liu, Tong Ma, Chengyu Cao, and Xingwei Wang, 2016, "3D Temperature Field Reconstruction Using Ultrasound Sensing System," SPIE.

[19] Mayer, A. M., 1873, "On an Acoustic Pyrometer," London, Edinburgh and Dublin Philosophical Magazine and Journal of Science, **45**, pp. 18–22.

[20] Schmidt, P. L., Greg Walker, D., Yuhas, D. J., and Mutton, M. M., 2014, "Thermal Measurements Using Ultrasonic Acoustical Pyrometry," Ultrasonics, **54**(4), pp. 1029–1036.

[21] Praher, B., Straka, K., and Steinbichler, G., 2013, "An Ultrasound-Based System for Temperature Distribution Measurements in Injection Moulding: System Design, Simulations and Off-Line Test Measurements in Water," Meas. Sci. Technol., **24**(8), p. 084004.

[22] Shen, X., Xiong, Q., Shi, W., Liang, S., Shi, X., and Wang, K., 2015, "A New Algorithm for Reconstructing Two-Dimensional Temperature Distribution by Ultrasonic Thermometry," Math. Probl. Eng., **2015**, pp. 1–10.

[23] Bramanti, M., Salerno, E. A., Tonazzini, A., Pasini, S., and Gray, A., 1996, "An Acoustic Pyrometer System for Tomographic Thermal Imaging in Power Plant Boilers," IEEE Trans. Instrum. Meas., **45**(1), pp. 159–167.

[24] Massignan, J. P. D., Neves-Jr, F., Ofuchi, C. Y., Arruda, L. V. R., da Silva, M. J., and Morales, R. E. M., 2014, "Broadband Ultrasound Attenuation Technique

Applied to Two Phase Flow Pattern Recognition," J. Control Autom. Electr. Syst., **25**(5), pp. 547–556.

[25] Samet, N., Maréchal, P., and Duflo, H., 2011, "Ultrasound Monitoring of Bubble Size and Velocity in a Fluid Model Using Phased Array Transducer," NDT E Int., **44**(7), pp. 621–627.

[26] Chakrapani, S. K., 2017, "Nonlinear Laminated Plate Theory for Determination of Third Order Elastic Constants and Acoustic Nonlinearity Parameter of Fiber Reinforced Composites," Compos. Struct., **180**, pp. 276–285.

[27] Bermes, C., Kim, J.-Y., Qu, J., and Jacobs, L. J., 2007, "Experimental Characterization of Material Nonlinearity Using Lamb Waves," Appl. Phys. Lett., **90**(2), p. 021901.

[28] Schmerr, L. W., 1998, *Fundamentals of Ultrasonic Nondestructive Evaluation: A Modeling Approach*, Plenum Press, New York.

[29] Sia, T. F., Liu, X. L., Chiu, W. K., and Paton, R., 2002, "Glass Transition and Viscoelastic Behaviour of Partially Cured Composites," Compos. Struct., **57**(1–4), pp. 489–493.

[30] Maffezzoli, A., Quarta, E., Luprano, V. a. M., Montagna, G., and Nicolais, L., 1999, "Cure Monitoring of Epoxy Matrices for Composites by Ultrasonic Wave Propagation," J. Appl. Polym. Sci., **73**(10), pp. 1969–1977.

[31] Lionetto, F., and Maffezzoli, A., 2013, "Monitoring the Cure State of Thermosetting Resins by Ultrasound," Mater. Basel, **6**(9), pp. 3783–3804.

[32] Lionetto, F., Tarzia, A., and Maffezzoli, A., 2007, "Air-Coupled Ultrasound: A Novel Technique for Monitoring the Curing of Thermosetting Matrices," IEEE Trans. Ultrason. Ferroelectr. Freq. Control, **54**(7), pp. 1437–1444.

[33] Sun, Z., Cheng-Kuei, J., Yan, J., and Ming-Yuan, C., 2005, "Application of Ultrasound and Neural Networks in the Determination of Filler Dispersion During Polymer Extrusion Processes," Polym. Eng. Sci. Newtown, **45**(6), pp. 764–772.

[34] Hæggström, E., and Luukkala, M., 2000, "Ultrasonic Monitoring of Beef Temperature During Roasting," LWT - Food Sci. Technol., **33**(7), pp. 465–470.

[35] Tong Ma, Yuqian Liu, Chengyu Cao, Jingcheng Zhou, Nan Wu, and Xingwei Wang, 2015, "3D Reconstruction of Temperature Field Using Gaussian Radial Basis Functions (GRBF)," Lijiang, China.

[36] Liu, S., Liu, S., and Ren, T., 2016, "Ultrasonic Tomography Based Temperature Distribution Measurement Method," Measurement, **94**, pp. 671–679.

[37] Motchenbacher, C. D., and Connelly, J. A., 1993, *Low Noise Electronic System Design*, J. Wiley & Sons, New York.

[38] Ehrenstein, G. W., and Theriault, R. P., 2001, *Polymeric Materials: Structure, Properties, Applications*, Hanser ; Hanser Gardner Publications, Munich : Cincinnati, OH.

[39] Barry, T., Kesharaju, M., Nagarajah, C., and Palanisamy, S., 2016, "Defect Characterisation in Laminar Composite Structures Using Ultrasonic Techniques and Artificial Neural Networks," J. Compos. Mater., **50**(7), pp. 861–871.